Genome-Scale Dynamic Modeling of the Competition Between *Rhodoferax* and *Geobacter* in Anoxic Subsurface Environments

by

Kai Zhuang

A thesis submitted in conformity with the requirements

for the degree of Masters of Applied Science

Graduate Department of Chemical Engineering

University of Toronto

Abstract

Thesis Title:	Genome-scale Dynamic Modeling of the Competition Between *Rhodoferax* and *Geobacter* in Anoxic Subsurface Environments
Degree:	Masters of Applied Science (MASC)
Convocation Year:	2010
Name:	Kai Zhuang
Department:	Chemical Engineering and Applied Chemistry
University:	University of Toronto

In situ bioremediation by Fe(III) reducers is a strategy for clean-up of ground water through reductive immobilization. The dynamics of the community involved is complex and needs to be understood better for improving the bioremediation. Here, we have created a dynamic genome-scale metabolic model of *Geobacter sulfurreducens* and *Rhodoferax ferrireducens*, the two primary iron-reducers in subsurface environments, in order to understand the community competition prior to and during uranium-bioremediation. The simulation results suggest that the community competition is modulated by two factors: the ability of *G. sulfurreducens* to fix nitrogen under ammonium limitation, and a rate vs. yield trade-off between these two organisms. This model will be an important tool for the analyses of more complex microbial communities and the design of effective uranium-bioremediation strategies.

Acknowledgements

This research was supported by the Office of Science (BER), U.S. Department of Energy, Cooperative Agreement No. DE-FC02-02ER63446 and Grant No. DE-FG02-07ER64367, as well as Canada Foundation for Innovation and University of Toronto Open Fellowship. Special thanks: Caitlin O'Connell for her artistic illustration, Laurence Yang for his insightful discussions, and Emma Janssen for her grammatical corrections. Special thanks: Radhakrishnan Mahadevan for being a supportive, understanding, and talented supervisor.

Table of Contents

List of Figures

Chapter 1. Modeling Uranium Bioremediation

1.1 *In Situ* Uranium Bioremediation

Uranium is a contaminant posing serious health risks to our society. The source of this contamination can be traced to weapon testing wastes and mill tailings, which releases U(VI) to the subsurface. The contaminant is often carried by groundwater flow to a river system, leading to significant environmental concern. Traditional remediation technologies are limited by contaminant volume and process efficiency. The discovery of several uranium-reducing microorganisms, such as *Geobacter sulfurreducens*, *Geobacter metallireducens*, and *Desulfovibrio vulgaris*, gave rise to a novel uranium treatment technology – microbial-mediated uranium immobilization, or *in situ* uranium bioremediation. By artificially introducing appropriate substrates into the contaminated subsurface, this technology promotes the growth and reductive activities of pre-existing uranium-reducing microorganisms in the subsurface. The reduction of U(VI) to U(IV) leads to the precipitation of uranium, hence immobilizing it within the subsurface. This immobilization prevents spread of uranium contamination.

The US Department of Energy has recognized microbial-mediated uranium bioremediation as a novel method with great potential, and created several test sites for studying uranium bioremediation. However, it was found that uranium bioremediation is an extremely complex process influenced by a combination of several factors including geochemistry, transport, and microbial activities [6]. Therefore, computational models of

the geochemistry, transport, and microbial activities of the uranium-contaminated subsurface environment are required for designing effective bioremediation strategies. The Rifle *in situ* bioremediation test site in Colorado is thought to be significantly influenced by microbial activity [7], therefore, we focus on studying the microbial community activities prior to and during bioremediation.

1.2 Overall Project Motivation

A wide phylogenetic diversity of microorganisms that are capable of dissimilatory metal reduction has been recovered from subsurface environments [8, 9]. The factors controlling which species dominate in a given subsurface environment are poorly understood, but may have important environmental consequences. For example, some dissimilatory metal-reducing microorganisms such as those from the *Geobacteraceae* family are capable of reducing U(VI) to U(IV), which impacts the mobility of uranium in the subsurface [8-14]. Stimulating dissimilatory metal reduction in order to promote the reductive precipitation of uranium shows promise as a bioremediation strategy for uranium-contaminated groundwater [7, 15], but relies on stimulating the appropriate dissimilatory metal-reducing microorganisms.

During uranium bioremediation field experiments at the Rifle site in Colorado, acetate is injected into the subsurface to promote the growth and activities of *Geobacter* species. However, it was found that several non-uranium-reducing organisms, including *Rhodoferax* species and acetate-oxidizing sulfate reducers, compete against *Geobacter* species for this substrate (Figure 1-1) [7, 15, 16]. It has been proposed that competition from these organisms affects the long-term viability of current bioremediation strategies, which is evident from a decrease in the relative abundance of *Geobacter* species after 50 days of acetate injection [7, 15, 16].

The overall motivation of our project, which this Masters of Applied Science research project is a part of, is to develop effective uranium bioremediation strategies. In particular, we are interested in overcoming the long-term viability issue of the current

bioremediation strategies. The bioremediation process at Rifle is highly complex due to the dynamic interactions between multiple microbial and metabolic species. Given the complexity of the problem, we have decided to approach the problem by first developing a computational model of the subsurface community metabolism, and then use the model to investigate the phenomena during bioremediation, and finally use the model to aid in our design of novel bioremediation strategies.

This thesis documents a sub-project of this project that focuses on the competitive interactions between *Geobacter* and *Rhodoferax* species (Figure 1-1). It is intended as a pilot project that develops and refines the modeling approach by focusing on a small but important sub-community of the more complex overall community.

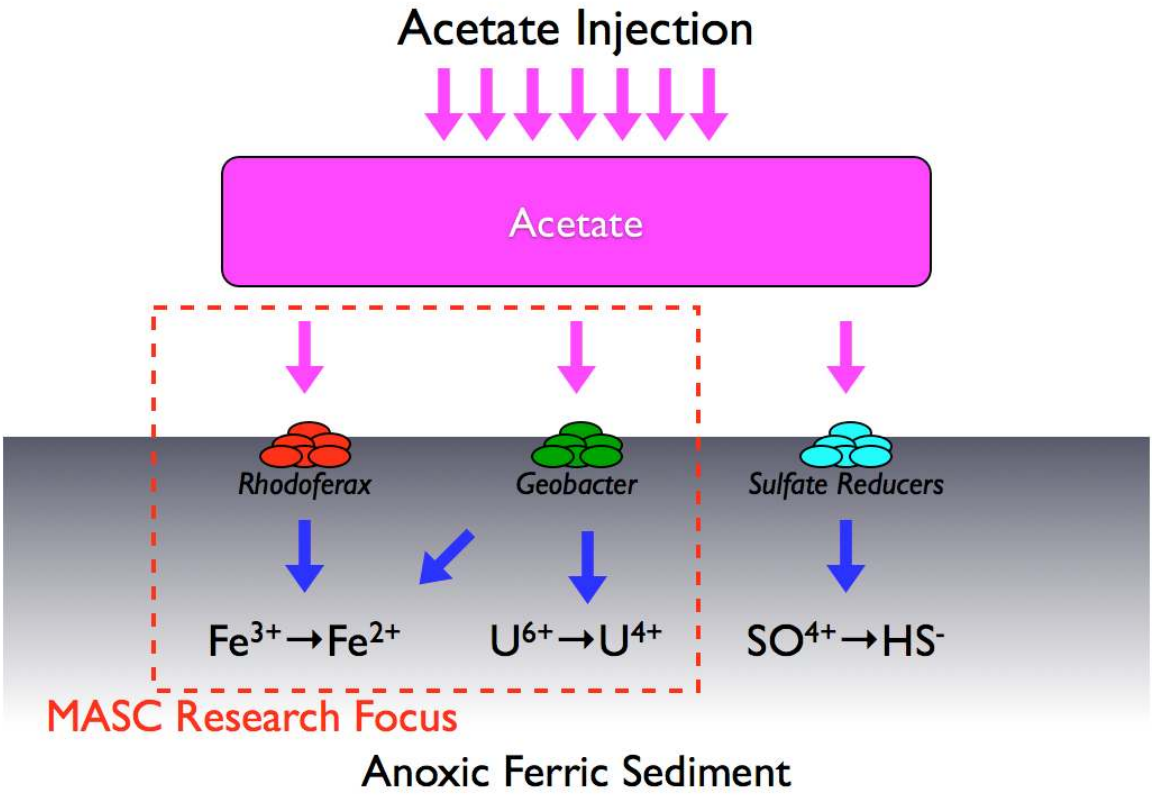

Figure 1-1. Microbial Competition at Rifle During Uranium Bioremediation

During the *in situ* uranium bioremediation experiments at the Rifle site, injected acetate is competitively utilized by *Geobacter*, *Rhodoferax*, and sulfate-reducing species as electron donor. The MASC project described in this thesis focuses on the interactions between *Geobacter* and *Rhodoferax* species. *Geobacter* simultaneously reduces U(VI) and Fe(III), where as *Rhodoferax* is only capable of Fe(III) reduction. Since Fe(III) is the primary electron acceptor responsible for *Geobacter* growth as the concentration of Fe(III) is three orders higher than that of U(VI), *Rhodoferax* essentially competes with *Geobacter* for both electron donor and acceptor. This makes understanding the competition between these two organisms essential for developing effective uranium bioremediation strategies.

1.3 *Geobacter* and *Rhodoferax* competition at Rifle

Field investigations of in situ uranium bioremediation at the Rifle site have demonstrated that *Rhodoferax* and *Geobacter* species, two phylogenetically distinct groups of dissimilatory metal-reducing microorganisms, are important components of the naturally anoxic subsurface at this site [16]. Multiple field experiments at the Rifle site have demonstrated that when dissimilatory metal reduction is artificially stimulated with the addition of acetate to the subsurface, *Geobacter* consistently become the predominant dissimilatory Fe(III) reducing microorganisms[7, 17]. This is despite the fact that like *Geobacter* species [9, 18, 19], the one described Fe(III)-reducing *Rhodoferax* species, *Rhodoferax ferrireducens*, is also capable of oxidizing acetate with the reduction of Fe(III) [20]. However, in contrast to the *Geobacter* species, *R. ferrireducens* has not been shown to be capable of U(VI) reduction, and in addition cannot fix nitrogen in the absence of ammonium [20] (Figure 1-2). Therefore, the ability of *Geobacter* species to outcompete *Rhodoferax* species may be critical for the success of stimulated in situ bioremediation at the Rifle site, and presumably other similar uranium-contaminated environments. The relative abundance of *Rhodoferax* and *Geobacter* species in different subsurface locations within the site has been measured, the competition among these Fe(III) reducers appeared to be related, at least in part, to the availability of ammonium in those locations [16] (Figure 1-2C).

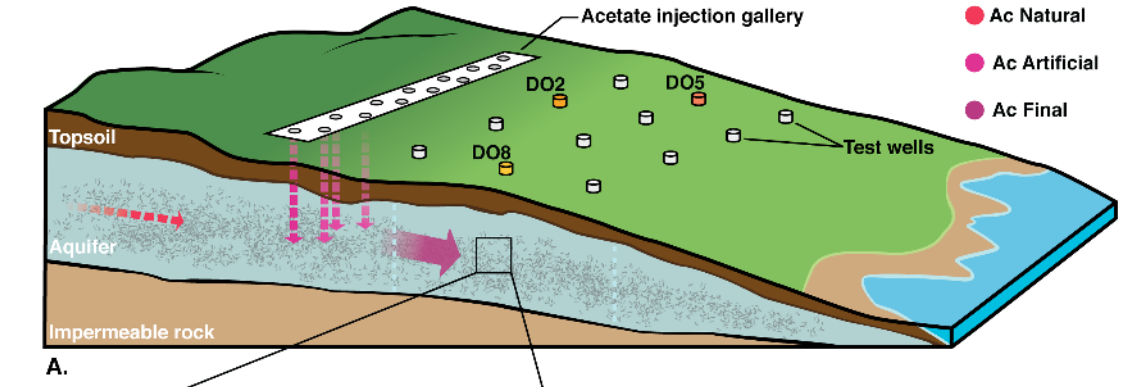

A.

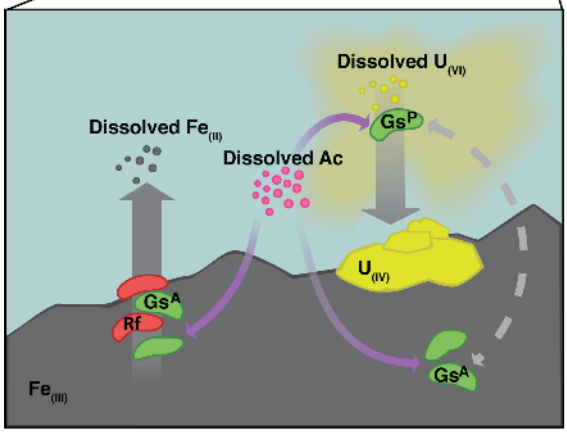

B.

	Day	Average [NH4+]	[NH4+] at Day 0	*Geobacter*	*Rhodoferax*	*Geobacter* fraction
DO2	0			7	5	58%
	9	70 µM	40 µM	77	0	100%
	18			72	2	97%
DO5	0			7	4	64%
	9	7 µM	21 µM	96	0	100%
	14			78	0	100%
DO8	0			6	24	20%
	9	300 µM	400 µM	78	5	94%
	18			53	0	100%

C.

Figure 1-2. Conceptual Model of Uranium Bioremediation

A) Prior to acetate injection, acetate is generated in the subsurface primarily through fermentation. During bioremediation, acetate is injected to the subsurface at high concentrations through the injection galleries. The artificial flow of acetate is combined with natural acetate flow, and follows the direction of the ground water. This acetate stimulates the growth of multiple microbial species downstream of the injection galleries, including *Geobacter* and *Rhodoferax* species. Groundwater samples are collected periodically at the test wells downstream of the injection galleries, including wells D02, D05, and D08. Various tests were performed on these groundwater samples, including ammonium concentration measurements and 16S rRNA based analysis of the relative microbial abundance.

B) Both *Geobacter* and *Rhodoferax* oxidize the dissolved acetate, and carry out the reduction of Fe(III) by attaching to a ferric iron surface. *Geobacter* is also capable of reducing U(VI) in its planktonic phase. Given that Fe(III) is the primary electron acceptor for *Geobacter*, this implies that the organisms compete for both electron donor and acceptor. The reduction of Fe(III) creates dissolved Fe(II), while the reduction of dissolved U(VI) creates U(IV), which precipitates. The reductive precipitation of uranium effectively removes uranium from the groundwater.

Rf : *Rhodoferax*
Gs^A : *Geobacter* (attached to sediment)
Gs^P : *Geobacter* (planktonic)

C) Ammonium concentrations at wells D02, D05, and D08 are measured periodically. Here, the initial and average ammonium concentration is shown. The *Geobacter* and *Rhodoferax* columns show the number of *Geobacter* and *Rhodoferax* 16S rRNA genes as a percentage of the total number of 16S rRNA genes in the sample. *Geobacter* fraction is calculated using Eq. X. The relative abundance of these two organisms appears to be related to the concentration of ammonium.

1.4 Need for a Community Metabolic Model

In order to develop effective and long-term viable bioremediation strategies, it is critical for us to understand the mechanism of the competition between *Geobacter* and *Rhodoferax* species, as well as predicting the outcome of the competition. Traditional modeling techniques such as Monod-type kinetic models and its derivatives [21] are limited by inaccurate predictions when applied to complex environments involving multiple metabolites. Genome-scale metabolic modeling offers the possibility of predicting the physiological responses of microorganisms to a diversity of environmental conditions as well as the interactions of microorganisms with each other and their environments [22, 23]. Flux Balance Analysis (FBA) models of pure cultures, such as *Escherichia coli* [24-28] and *G. sulfurreducens* [3, 29] are capable of predicting the detailed physiology including growth yields and respiration rates. This modeling approach has been useful for both understanding the behavior of biological systems in complex environments and for engineering purposes [30-35].

The availability of the genome sequences of *Geobacter* [36, 37] and *Rhodoferax* [4] provides the opportunity to apply FBA to examine the interaction and competition between *Geobacter* and *Rhodoferax* species under naturally occurring and artificially stimulated Fe(III)-reducing conditions. However, the *Geobacter* and *Rhodoferax* community is highly complex, involving multiple microbial and metabolic species, and the concentrations of these species are highly dynamic. Currently, there are no metabolic modeling techniques capable of dynamically simulating such complex systems. In order to model the microbial community of interest, we need to develop a community metabolic modeling framework capable of handling such complexity.

1.5 Thesis Objective

This thesis is motivated by our need to develop effective and long-term viable bioremediation strategies. In particular, we aim to use computational modeling to understand the mechanism of the competition between *Geobacter* and *Rhodoferax* species, as well as predicting the outcome of the competition. As pointed out in the previous section, there are no computational modeling techniques that are applicable to this community. Therefore, this thesis has two objectives:

1. To develop a **general** *computational framework* applicable to complex (dynamic, multi-species) microbial communities.
2. To apply this *computational framework* to the investigation of the *Geobacter* and *Rhodoferax* microbial community in uranium-contaminated subsurface. In particular, we aim to answer the following two questions:
    a. Why do two acetate-oxidizing iron-reducing organisms occupy the same niche?
    b. Will the existence of *Rhodoferax* species affect the outcome of uranium bioremediation?

Chapter 2. Metabolic Modeling

2.1 Systems Biology and Metabolic Modeling

The past decade has seen an exponential growth in the field of systems biology, particularly in the area of modeling large-scale biochemical networks. Systems biology has greatly increased our understanding of the complex processes of life and has become an indispensable tool for metabolic and bioprocess engineering. The advent of systems biology is fueled by the recognition of the limitation of the reductionist paradigm. Systems biology adopts a holistic view of biological systems; its approach allows the investigation of systemic features, including emergence, robustness, and modularity [38-41].

One prominent systems biology method used for the analysis of metabolic networks is the constraint-based modeling. The model has two major components - the stoichiometric matrix and the constraints [42] (Figure 2-1). The stoichiometric matrix is a mathematical representation of the biochemical reaction network, and the constraints represent physiological and environmental limitations on the network. Generally, the biochemical reaction network is underdetermined - by applying additional constraints, we reduce the size of the solution space [40, 42, 43] (Figure 2-1). Because this approach does not require any kinetic descriptions, a constraint-based model (CBM) can be constructed with minimal experimental data. On the other hand, physiological information can be described by a mathematical constraint [40, 42, 43]. A standard model reconstruction process has been described [40] and can be automated to aid the manual reconstruction process [37, 44]. To date, 46 genome-scale metabolic models have been successfully reconstructed [40, 45], including both well studied organisms such as *Escherichia coli*

[25-28, 40, 45], *Saccharomyces cerevisiae* [46], as well as less studied organisms including *Geobacter sulfurreducens* [29, 47], *Geobacter metallireducens* [37], *Rhodoferax ferrireducens* [4], and *Dehalococcoides sp*.[48].

Traditionally, constraints are defined by experimental observations such as the maximum substrate uptake rate. Flux variability analysis can be used to computationally determine the non-viable solution space [49]. Michaelis-Menten kinetics can be used to incorporate kinetics measurements as dynamic constraints [50]. Recently, several novel methods have been developed to further reduce the solution space. Yang *et al.* analyzed experimentally determined competition fitness scores between knockouts using a bi-level optimization algorithm (the optimal capacity constraint identification algorithm, OCCI) to determine additional enzyme capacity constraints [51]. Henry *et al.* (2007) used group contribution theory to estimate the ΔG of metabolic reactions, and developed the thermodynamics-based metabolic flux analysis (TMFA) method, which includes both pathway flux constraints and thermodynamic constraints [52]. The relationship between the stoichiometric matrix and various constraints is graphically represented in Figure 2-1.

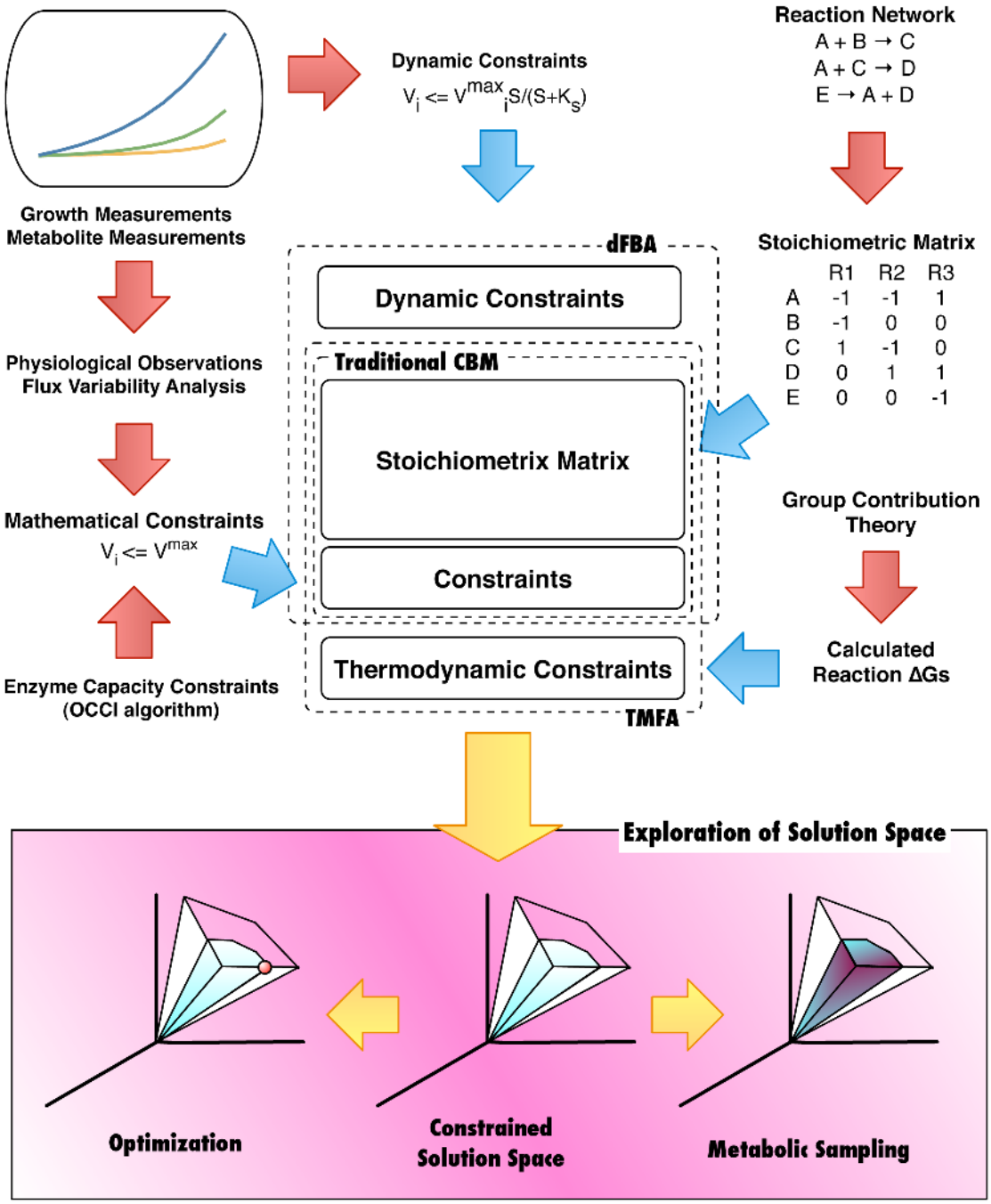

Figure 2-1. Constraint-Based Metabolic Modeling.

The primary components of constraint-based metabolic models include the stoichiometric matrix and the flux constraints. The stoichiometric matrix is a mathematical representation of the metabolic reaction network. The flux constraints can be directly measured through experiments, computationally derived using flux variability analysis, or inferred using the OCCI algorithm. The solution space can be explored using either optimization methods or metabolic sampling methods.
This figure is inspired by the graphics in several review papers from Dr. Palsson's Lab [40, 42, 43].

2.2 Exploration of Solution Space

Since constraint-based metabolic models are under-determined mathematically, it offers us a solution space instead of a single solution. Although there are many different methods to explore this solution space, these generally fall under the categories of optimization-based methods and stochastic-sampling based methods. Of the two, optimization-based methods are much more common.

Optimization-Based Methods

Optimization-based methods utilize mathematical programming techniques to select the optimal point in the solution space for a given objective function. For metabolic engineering purposes, this objective function often takes the form of maximizing or minimizing a particular flux of interest. Multiple fluxes can be maximized simultaneously; multi-level and multi-stage optimization has been used for metabolic and bioprocess engineering purposes as well [31, 34, 35]. These methods offer us insights on how to genetically modify an organism to achieve our engineering goals.

For the purpose of predicting metabolic behaviors, the objective function is a mathematical representation of the true cellular objective. The rationale behind this exercise is that under a constant environment, organisms tend to develop an optimal evolutionary strategy to cope with the environment. The most common method in this category is flux balance analysis (FBA). In FBA, the maximization of the biomass flux is used as the objective function. It was shown that by long-term exposure to a non-native steady-state environment, such as growth on glycerol, *E. coli* could be adaptively evolved

to exhibit the phenotypes of the FBA optimal solution [24]. Flux balance analysis (FBA) models for pure cultures such as *Escherichia coli* and *Geobacter sulfurreducens* are capable of accurate growth predictions [3, 25, 26, 28, 53] as well as gene-expression predictions [54, 55]. While FBA is useful for organisms under long-term evolution, Minimization of Metabolic Adjustment (MoMA) and Regulatory On/Off Minimization (ROOM) are useful for the prediction of metabolic behaviors of knock-out strains. MoMA minimizes the difference between the metabolic distributions of wild-type and knock-out organisms [56], where as ROOM minimizes the number of significant metabolic changes between wild-type and knock-out organisms [57].

What is the *Right* Objective Function?

Despite the success of FBA in growth yield predictions, there is a great amount of confusion on its physiological significance, as well as criticism on its universality. The maximization of the biomass flux in FBA is often quoted as the maximization of growth rate [27, 28, 40, 42, 43, 58]. However, Schuster *et al.* suggested that in practice, FBA maximizes biomass rate for a fixed substrate uptake rate, which should be interpreted as maximization of molar yield under carbon limiting conditions. The authors compared this approach to the maximization of reaction rate, and suggested that the optimal solution produced by FBA is not always favored by evolution due to a well-studied trade-off between rate and biomass yield [59].

The crux of this argument is that from a game-theory perspective, the true cellular objective in a competitive environment is the maximization of growth rate, which is the product of substrate utilization rate and biomass yield ($\mu = v \cdot Y$). A mole of substrate

contains a fixed amount of Gibbs free energy (ΔG), which can either drive the rate of chemical reactions through entropic dissipation or be converted to biomass. This enforces a thermodynamic trade-off between biomass yield and the substrate utilization rate. In order to maintain internal steady state, substrate utilization rate is equal to substrate uptake rate under most conditions. In other words, an organism must optimize either energetic efficiency or substrate uptake rate. Since life exists under the realm of non-equilibrium thermodynamics, the exact nature of this trade-off cannot be easily formulated mathematically. However, using a linear approximation, Pfeiffer *et al.* showed that rate optimizers are favored if the feed rate is high, and yield optimizers are favored if the feed rate is low [60]. The existence of this trade-off is supported by experimental studies [61].

It is important to note that the optimization in FBA operates at the **pathway level** alone, and should be interpreted as the maximization of specific growth rate **given** a fixed substrate uptake rate **and** a fixed stoichiometric matrix. For example, in *E. coli*, much more ATP can be produced from glucose through the respiratory pathway than the fermentative pathway. Given fixed glucose and oxygen uptake constraints, the current FBA formulation correctly predicts that if oxygen is in excess, all glucose will be processed through the respiratory pathway, but if oxygen is limited, both respiratory and fermentative pathways are used, thus maximizing growth rate at the expense of growth yield. The current FBA objective function is a good approximation to the maximal growth rate at the pathway level; however, it does not take into consideration the cost of enzyme and metabolite production, which can be important at higher substrate uptake rates [62, 63].

The energetic efficiency of a metabolic model is fixed by the stoichiometry of the electron transport chain. Because mutations can potentially occur in the electron transport chain, this can limit the universality of FBA. For example, *E. coli* and *B. subtilis* strains have different versions of electron transport chains, each with different energetic efficiencies. Maharjan *et al.* found that a single strain of *E. coli* in a chemostat can evolve into up to nine different strains with very different phenotypic and metabolic characteristics, and not all phenotypes correspond to the optimal growth rate produced by FBA [64]. In order to reflect this trade-off in systems biology models of metabolism, thermodynamics must be taken into account. Although TMFA is a step forward in this direction [52], it only incorporates thermodynamics inside the constraints, not the objective function. Other approaches that investigate this further are needed.

Size, Shape, and Distribution of Solution Space

The concern of Maharjan *et al.* over metabolic diversity is not unfounded, since redundancy in metabolic pathways is well noted [41, 64]. It is often important to know the size and shape of the solution space, as well as the distribution of the solutions within this space. The analysis of extreme pathways and elementary modes can help determine the shape of the solution space [65, 66], while stochastic sampling can be used to determine the distribution of viable solutions [41, 66, 67]. One of the key benefits of the stochastic metabolic sampling method is that we can investigate the solution space where the biomass flux is within a certain percentage of the FBA optimal solution, and thereby, recognizing the reality of metabolic diversity. For example, in the Maharjan paper, the growth rates of most mutants are within 15% of the maximum growth rate [64]. These

methods can also explore the effect of mutation on the solution space. The sampling of solution space has been extensively studied for various metabolic networks including the Red Blood Cell Network [68, 69] and *E. coli* central metabolism [66].

2.3 Computational Challenges of Modeling Uranium Bioremediation

An important area of applications of constraint-based metabolic models is environmental biotechnology, particularly subsurface bioremediation. The process of subsurface bioremediation is extremely complex, involving physical, chemical and biological factors. An approach of relying solely on experimental studies is normally time-consuming and unable to adequately describe effects of various factors on this process. The coupling of detailed experimental studies with mathematical models are therefore rapidly becoming a widely used approach to effectively evaluate subsurface contamination problems and to design and formulate appropriate bioremediation strategies (Figure 2-2).

However, there are significant challenges in mathematically modeling the metabolism of the complex microbial communities involved in bioremediation. For example, the uranium bioremediation at the Rifle site involves a host of different microbial species – multiple species from the *Geobacteraceae*, *Rhodoferax ferrireducens*, and sulfate reducing bacteria from at least two different families all plays important roles in the bioremediation process. In addition, these organisms interact with each other by competing for and exchanging metabolites in the environment. Important metabolites to this community include (but are not limited to): acetate, ferric iron, ferrious iron, sulfate, dissolved uranium, ammonium, dissolved nitrogen, carbon dioxide, and water. This is a highly complex problem and there are no modeling techniques that can adequately handle problems of this complexity. Traditional modeling techniques such as Monod-kinetic equations cannot yield accurate prediction of the community metabolism at this complexity, and currently, most constraint-based metabolic modeling techniques are

mostly focused on single cultures. The next section describes several pioneer attempts at extending CBMs to the community realm, and discusses the reason that these attempts are inadequate for complex problems such as bioremediation.

2.4 Extending CBMs to Microbial Communities

CBMs of microbial metabolism have focused on pure cultures in the past. However, microorganisms in nature exist in complex communities, either in cooperation or in competition. The composition of the community and the metabolic states of its members are highly sensitive to the ever-changing environment. Furthermore, community activities can modify their environment, which further modifies community composition and behavior. For example, the rumen microbial community composition varies significantly based on the host's dietary input [70], and the community's digestive performance is decided by the community's composition. Given that "microbes comprise nearly half of all biomass on earth" [71], one cannot truly understand environmental dynamics without understanding microbial communities. The advent of systems biology has greatly increased our understanding of the complex processes at the organism level. The same approach can be applied to microbial ecology, with additional complexities. Both living and abiotic processes, including chemical, biological, and transport phenomena, must be modeled. Such models can elucidate the intricate interactions and emergent properties of the entire system [71].

There have been several pioneer attempts at extending the constraint-based modeling paradigm to the modeling of microbial communities, however, the methods used in these attempts are inadequate for complex (dynamic, multi-species) systems such as the microbial community relevant to subsurface bioremediation.

Vallino (2003) has modeled a rumen microbial consortium as a distributed network constrained by thermodynamics to test the hypothesis that maximization of the rate of

energy dissipation is the objective function for the microbial community. However, the metabolism of each organism is represented by a single reaction in this model, therefore physiological details cannot be incorporated into the model [72].

Stolyar et al. (2007) created the first metabolic model of a mutualistic microbial community by directly connecting the FBA models of *Desulfovibrio vulgaris* and *Methanococcus maripaludis* [73]. The authors assumed that the species are interdependent, thereby justifying their usage of a constant biomass flux ratio as the objective function. Another caveat of this model is that it cannot predict the dynamic shifts in population and their metabolite concentrations. While this approach may be appropriate when the microorganisms are inter-dependent, it is inappropriate in ecological settings where the community composition is dynamic. Nonetheless, this is a noteworthy attempt at extending systems biology for modeling microbial community metabolism.

To accurately predict the metabolic behavior of a dynamic microbial community involving multiple microbial and metabolic species, a novel computational framework is required. With modeling uranium bioremediation in mind, we have set the design criteria for such computational framework to be:

1. The framework should be able to integrate existing metabolic models of single organisms into a community metabolic model with *relative ease*.
2. The framework should be able to model the *dynamic* behavior of *multiple* microbial and metabolic species in a given environment.

3. The model predictions should be accurate and detailed enough to aid both the investigation of uranium-contaminated subsurface microbial community and the designing of effective bioremediation strategies.

Based on the above design criteria, we have developed the Dynamic Multi-species Metabolic framework (DMMM). The rest of this document will describe this novel computational framework in detail, as well as the application of this framework to the investigation of the competition between *Geobacter sulfurreducens* and *Rhodoferax ferrireducens*.

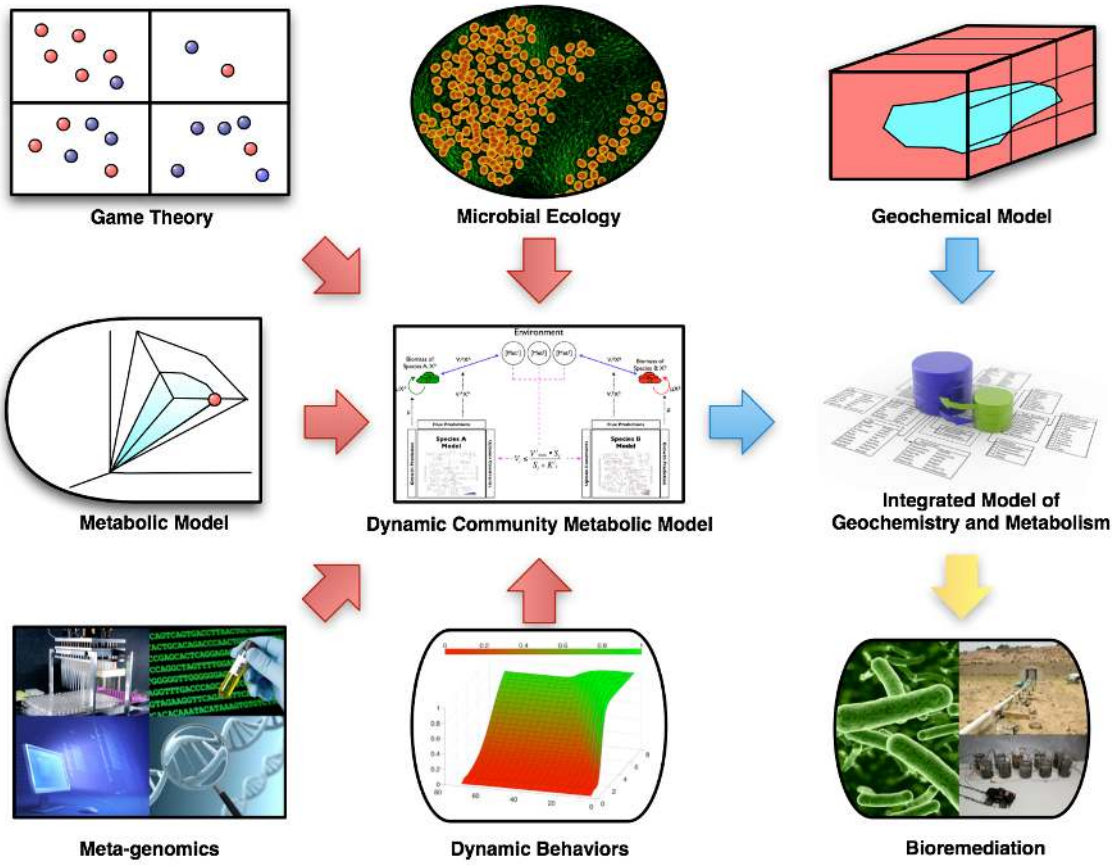

Figure 2-2. Applying Constraint-Based Modeling to Bioremediation

The application of systems biology for environmental biotechnology purposes requires the integration of geochemical modeling and community metabolic modeling. The community metabolic model should be based on the constraint-based metabolic model, but incorporating concepts of game theory, microbial ecology, dynamic modeling, as well as meta-genomic data. This thesis focuses on the development of the dynamic community metabolic model of uranium bioremediation. However, to fully understand bioremediation, this model needs to be integrated with geochemical model of the uranium-contaminated subsurface.

Chapter 3. The Dynamic Multi-species Metabolic Modeling framework

3.1 The original FBA formulation and the dynamic FBA formulation

The Dynamic Multi-species Metabolic Modeling (DMMM) framework is based on the dynamic Flux Balance Analysis (dFBA) [50], an extension of the original FBA.

The original Flux Balance Analysis (FBA) is formulated as the following:

$$\begin{aligned} &\text{maximize } \mu = c^T v \\ &\text{subject to } Av = 0 \\ &\qquad v^{\min} \le v \le v^{\max} \end{aligned} \tag{1}$$

In this formulation, the objective of the linear program is the maximization of the growth rate, μ, calculated by $c^T v$, where c^T is the objection function column and v is the vector of reaction fluxes. This maximization of the objective function is subject to constraint Av = 0, which is a mathematical representation of the assumption that the cell is at steady state internally. Additional constraints in the form of $v^{min} \le v \le v$ can be applied to represent computationally or experimentally determined flux limitations.

Due to the limitation of the internal steady state assumption, the original FBA formulations cannot accurately predict cellular behaviors in highly dynamic processes, such as diauxic growth of *Escherichia coli*. The dynamic Flux Balance Analysis (dFBA) extends the original FBA formulation by linking the exchange fluxes and the biomass flux with the rate of change in the environmental metabolite concentrations and the biomass concentration. The dFBA is formulated as below:

$$\frac{dX}{dt} = \mu X$$
$$\frac{dS_i}{dt} = A_i v_i X$$

$$\text{Maximize } \mu = c^T v \qquad (2)$$
$$\text{subject to } Av = 0$$
$$v^{\min} \le v \le v^{\max}$$

$1 \le i \le$ to number of metabolites

By integrating over the metabolic rates and the growth rate, the dFBA formulation allows the dynamic prediction of changes in the biomass concentration and well as metabolite concentrations external to the cell. This is a great improvement over the original FBA in applications where the dynamic shifts in external metabolite concentrations determines the shifts in internal cellular states, such as diauxic growth of *Escherichia coli*[50]. However, the dFBA formulation is still restricted to single organisms.

3.2 The formulation of the DMMM framework

The Dynamic Multi-species Metabolic Modeling (DMMM) framework extends the dFBA formulation to the community realm. Mathematically, the DMMM framework can be formulated as:

$$\frac{dX_j}{dt} = \mu_j X_j$$
$$\frac{dS_i}{dt} = \sum^{j} A_i{}^j v_i{}^j X_j$$

$$\begin{aligned} &\text{Maximize } \mu_j = c^T v_j \\ &\text{subject to } A_j v_j = 0 \\ &\qquad v_j{}^{\min} \le v_j \le v_j{}^{\max} \end{aligned} \tag{3}$$

$1 \le i \le$ to number of metabolites
$1 \le j \le$ to number of microbial species

In this formulation, j indicates the ^{j}th species in the community. X_j is the biomass of the ^{j}th species in the community. A_j is the stoichiometric matrix of the ^{j}th species in the community; A_{ji} is ^{i}th row of the stoichiometric matrix of the ^{j}th species in the community. v_j is the reaction flux vector of the ^{j}th species in the community; v_{ji} is the reaction flux of the ^{i}th metabolic reaction of the ^{j}th species in the community. S_i is the ^{i}th metabolite in the environment. v_j^{max} and v_j^{min} are the maximum and minimum reaction flux vector of the ^{j}th species in the community; they can be acquired computationally using flux variability analysis or acquired experimentally. For the members of v_j^{max} and v_j^{min} corresponding to external metabolites, the uptake/production constraints to these fluxes can be calculated based on the environmental concentration of these metabolites, using

either the On/Off method or the Michaelis–Menten kinetics. For a sample of this algorithm, see Section 3.3.

By integrating the growth rates of all microbial species within the community, as well as the production/consumption rates of all metabolic species in the environment, the DMMM framework can dynamically predict the temporal changes in metabolite and biomass concentrations in a complex microbial community.

3.3 Sample implementation of the DMMM framework

Although the mathematical formulation of the DMMM framework was described in Section 3.2, it might be difficult to follow for those readers without background in mathematical programming and metabolic modeling. Therefore, a sample implementation of the DMMM framework is provided here (Figure 3-1). This sample implementation assumes the existences of a community consisting of two microbial species, A and B, and three substrates, Met^1, Met^2, Met^3. The numbers of microbial and metabolic species are arbitrary in this example. The maximal numbers of microbial and metabolic species depend on the limitation of the computational hardware.

After a simulation length (hrs) and a simulation step size (hrs) is given, this particular implementation of the DMMM framework execute the following routines during each simulation step:

R1: The concentration of Met^1, Met^2, and Met^3 are used to calculate the upper and lower constraints to v_1^A, v_2^A, v_3^A, v_1^B, v_2^B, and v_3^B, where v_i^j represent the ^{i}th reaction flux of the species j. Two calculation methods are commonly used:

i. On/Off methods

   if $[Met^i] > 0$, then $-\infty < v_i^j < \infty$

   if $[Met^i] <= 0$, then $v_i^j = 0$

j. Michaelis–Menten kinetics

$$V_{i,\text{constraint}} \le V_i^{\max} \bullet \frac{S_i}{S_i + K^i_s} \qquad (4)$$

R2: Solve two linear programs (FBA models of species A and B) to calculate the specific growth rates, μ^A and μ^B, as well as the reaction fluxes v_1^A, v_2^A, v_3^A, v_1^B,

v_2^B, and v_3^B. If the linear programs are feasible, then continue to routine R3. If the linear program corresponding to species j is infeasible, then a special cell-death routine RD is executed to calculate the rate of death r^d of the species j, and μ^j is set to r^d.

R3: The rate of change in the biomass of A and B are calculated with the equation:

$$\frac{dX^j}{dt} = \mu^j X^j \tag{5}$$

Calculate ΔX^j by integrating dX^j/dt over the simulation step.

Calculate the new X^j at the end of the simulation step with $X^{j\,new} = X^{j\,old} + \Delta X^j$.

R4: The rate of change in the concentration of external metabolite i is with the equation:

$$\frac{dS_i}{dt} = \sum^j v_i^j X_j \tag{6}$$

Calculate ΔS_i by integrating dS_i/dt over the simulation step.

Calculate the new S_i at the end of the simulation step with $S_i^{new} = S_i^{old} + \Delta S_i$.

Only the rates of change of external metabolites are integrated since all internal metabolites still follow the internal steady state assumption.

RD: The cell death RD routine is a special user-defined routine that is called upon when the environmental concentrations of substrates are insufficient to sustain the current biomass concentration of the organism. This routine is flexible and can be edited for each individual organism to reflect its specific mechanism of cell-decay. The RD routine produces the rate of cell death r^d, which should be considered a *negative* growth rate. After completion of RD, return to R3.

After routine R4 is completed, time advances one step-size. The routine R1 is initiated again. This continues until the simulation length is reached. This procedure is illustrated in Figure 3-1.

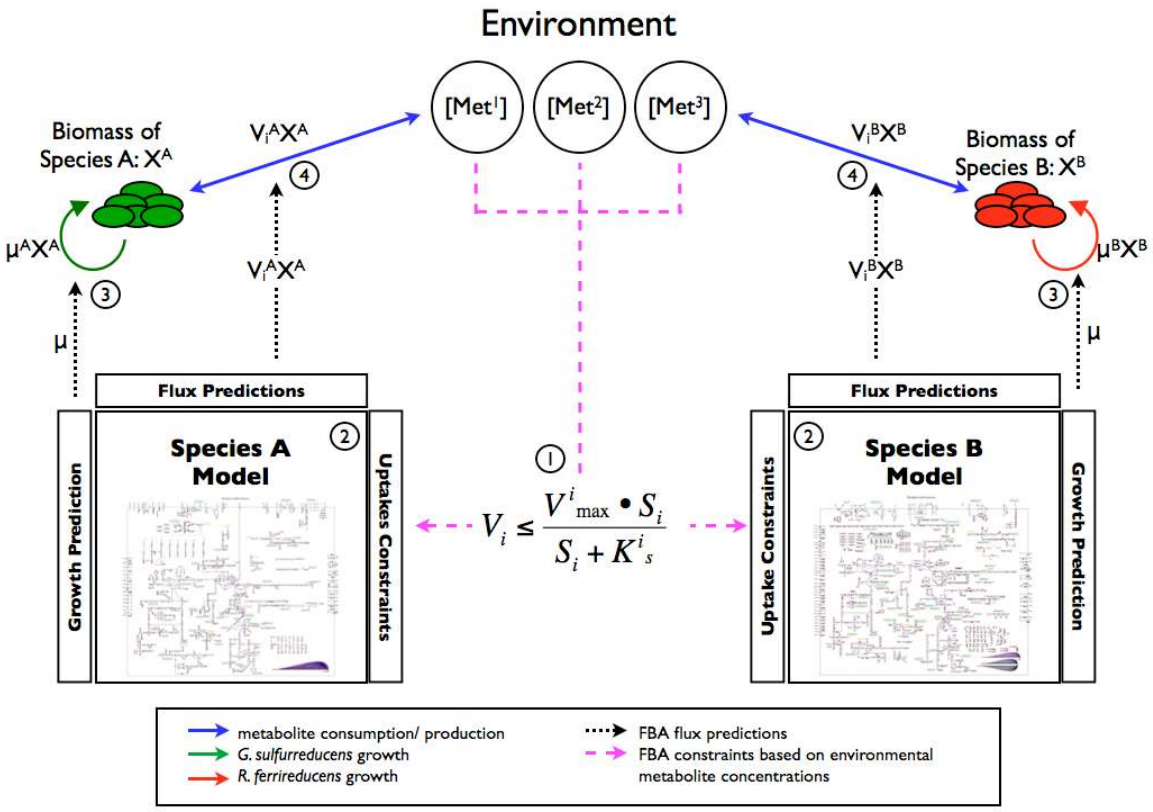

Figure 3-1. The Dynamic Multi-species Metabolic Modeling Framework

The DMMM framework consists of four major steps: [1] Calculation of the substrate uptake constraints based on current substrate concentration. [2] Solve the FBA problems for the member species of the community. This generates the specific growth rates and external reaction fluxes of the member species. If the FBA problem is infeasible for one or more of the member species, then a special cell-death simulation routine is used to generate the specific death rate. [3] Calculate dX/dt for each member species. Integrating over this rate to generate the dynamic profile of biomass concentrations. [4] Calculate dSi/dt for each member species. Integrating over this rate to generate the dynamic profile of metabolite concentrations.

3.4 Simulation of Cell-Death

The traditional way of modeling cell-death assumes that the death of microorganisms is often due to the failure to meet maintenance energy requirements [21, 74]. This assumption is reflected in the equation[21, 74]:

$$r^D = (q^S - m^S)Y \quad (7)$$

Here, q^S (mmol S/gDW/hr) is the uptake rate of substrate S, m^S (mmol S/gDW/hr) is maintainence requirement of substrate S (the uptake rate of substrate S required to maintain the current biomass), Y is the biomass yield on substrate S.

In metabolic models, the non-growth-related maintenance energy is represented with an ATP maintenance flux (m^{ATP}) with the unit mmol ATP/gDW/hr. To adapt Equation 7 to metabolic models, the limiting substrate S must be determined first. FBA is used to convert m^{ATP} to m^S by constraining the biomass growth flux to zero and minimize the uptake flux of S. Then, Y, the biomass yield on substrate S, is calculated using standard FBA. Finally, Equation 7 is used to calculated r^D (r^D is a negative number).

It is also important to note that in many situations, the community process of interest may not be sensitive to death rate. For example, the competition between *Geobacter* and *Rhodoferax* during uranium-bioremediation is insensitive to death rate. Therefore, in this case, the death rate calculation here is included for the sake of completeness only.

3.5 Implementation of DMMM framework in MATLAB

The mathematical formulation of the DMMM framework presented in the previous section has been implemented computationally in the MATLAB programming environment. Our implementation of the DMMM framework is designed to be an add-on to the COBRA Toolbox [75]. The COBRA Toolbox is a MATLAB toolbox (function library) designed for various metabolic modeling tasks. MATLAB is the standard tool of the engineering academia, and the COBRA toolbox aims to provide a standard computational method to complete metabolic modeling tasks. As an add-on to the COBRA Toolbox, the current implementation of the DMMM framework has can be easily integrated into the existing codes used by many academics. This will likely widen the impact of the DMMM framework.

To solve FBA linear programs, CPLEX solver is used. To connect CPLEX to MATLAB, the CPLEXINT interface is used (http://control.ee.ethz.ch/~hybrid/cplexint.php).

It is important to note that since there is an arithmetic solution to the ordinary differential equations (ODEs) corresponding to the rate of change of biomass and metabolite concentrations (Equation 5, Equation 6), our implementation of the DMMM does not require a numeric ODE solver. It is possible to implement the DMMM framework with a numeric ODE solver; however, this method would drastically reduce the computational speed without a significant increase in accuracy.

3.6 Advantage of the DMMM framework

The usage of the DMMM framework to model microbial communities holds significant advantages over the traditional Monod-kinetic models, the Stolyar community metabolic model [73] mentioned in section 2.4, as well as pure experimental methods.

DMMM vs. Monod-kinetic Model

The Monod-kinetic model can model relatively simple metabolism quite well. For example, if an organism is treated as having only one limiting substrate, S, then the organism's growth with respect to S can be modeled fairly accurately by:

$$\mu = \mu^{\max} \bullet \frac{[S]}{[S] + Ks} \tag{8}$$

If an organism is treated as having two limiting substrates, S1 and S2, then the organism's growth can be modeled with:

$$\mu = \mu^{\max} \bullet \frac{[S_1]}{[S_1] + K_{s_1}} \bullet \frac{[S_2]}{[S_2] + K_{s_2}} \tag{9}$$

For an organism with i limiting substrates, the organism's growth is modeled with the General Monod Model:

$$\mu = \mu^{\max} \bullet \prod_{1}^{i} \frac{[S_i]}{[S_i] + K_{s_i}} \tag{10}$$

For example, if we assume that each of the substrates are available at their saturation concentration (K_s), the Monod model would predict a growth rate of $1/2^n$ of the maximum, even though it is clear that the substrate concentrations are sufficient to allow the organism to grow at ½ the maximum. Moreover, the yield in the presence of multiple substrates needs to be experimentally determined for each combination, as there are no known mechanisms to compute the yields accurately for different metabolic states. Since

n is generally related to the metabolic complexity, the Monod-kinetic model does not scale up well with complex metabolisms. Realistically, prediction accuracy often becomes unacceptable when $i > 2$.

Since the DMMM framework is based on CBMs, it is capable of handling ***significantly*** more complex metabolisms. For example, the *Geobacter sulfurreducens* model [3] used in this thesis contains 727 reactions, 55 of which are exchange reactions ($i = 55$).

DMMM vs. Stolyar Model

Stolyar et al. published the first constraint-based metabolic model of a mutualistic microbial community in 2007[73]. In the Stolyar model, the CBMs of *Desulfovibrio vulgaris* and *Methanococcus maripaludis* are directly connected[73]. The authors assumed that the species are interdependent, thereby justifying their usage of a pair of arbitrary biomass flux weights (authors used 10:1, 1:1, 1:10) as the objective function[73]. This objective function is inappropriate for most microbial communities. Another caveat of this model is that it cannot predict the dynamic shifts in population and their metabolite concentrations. While this approach may be appropriate when the microorganisms are inter-dependent, it is inappropriate in ecological settings where the community composition is dynamic.

In comparison, the DMMM framework does not rely on arbitrary objective function – instead, the FBA problems representing each organisms are solved separately, allowing the usage of more established objective functions such as maximization of biomass flux. The DMMM framework is not restricted to mutualistic communities; it is capable of predicting the dynamic shifts in community composition and metabolites' concentration.

DMMM vs. Experimental Studies

While no model can ever achieve the accuracy of real experimental studies, usage of metabolic modeling has proved to be a valuable analytical tool [45]. The DMMM framework allows scientists to consider thousands of possible reactions and metabolites simultaneously, this together with necessary experimental work, can provide significant insights that are otherwise overlooked due to the limitation of the human brain. Furthermore, the DMMM framework allows scientists to observe the emergent properties of the complex microbial community, which are difficult (if not impossible) to predict without.

The DMMM framework allows complex experiments to be performed *in silico* prior to real experiments. These simulations can guide the formation of new hypothesis, which allows *in situ* and *in vivo* experiments to be performed selectively. This approach drastically decreases the cost and time required for discovery. Furthermore, this approach allows scientists to test otherwise difficult-to-prove hypothesis. For example, a scientist designing an environmental biotechnology strategy might want to study the effect of increasing groundwater flow rate, which would be very difficult to evaluate *in situ*.

Chapter 4. Methods

The previous chapter described the Dynamic Multi-species Metabolic Modeling (DMMM) framework, a novel *general computational framework* applicable to complex (dynamic, multi-species) microbial communities. This chapter described the **methods** we used to investigation of the *Geobacter* and *Rhodoferax* microbial community in uranium-contaminated subsurface.

4.1 Applying the DMMM framework to model the *Geobacter* and *Rhodoferax* community

The DMMM framework was used to evaluate competition between *Geobacter* and *Rhodoferax* species in anoxic environments in which Fe(III) is the primary electron acceptor available to these organisms. This represents conditions in uranium-contaminated subsurface environments, because Fe(III) is expected to be the predominant electron acceptor under anoxic conditions [10] and the concentration of U(VI) contaminants in the groundwater does not provide a significant source of electron-accepting capacity [20]. *Geobacter sulfurreducens* and *Rhodoferax ferrireducens* served as models for *Geobacter* and *Rhodoferax* species because genome-scale metabolic models of these organisms are available [4, 47]. The *G. sulfurreducens* model used is modified from the original published model [3], containing new reactions including an updated nitrogen-fixation stoichiometry. This model contains 727 reactions, 55 of which are exchange reactions. The published *R. ferrireducens* model [4] contains 822 reactions, 67 of which are exchange reactions. After applying the DMMM framework, the overall community model contains 85 external metabolites and two microbial species. The

temporal concentration profiles of all metabolites that are either secreted into or consumed from the environment and the biomass of the organisms in the community are calculated. The simulations were performed using the maximization of biomass yield as the cellular objective for both organisms [76, 77].

4.2 Kinetic parameters

As in the dynamic FBA (dFBA) formulation [50], dynamic constraints were applied to the flux of carbon and energy source, calculated using the Michaelis-Menten expression (Equation 4). The acetate transport kinetics of *G. sulfurreducens* have been determined by measuring [^{14}C]-labeled acetate uptake [5]. Three different acetate uptake mechanisms were found, each with different K_s saturation constants and specific uptake rates, V^{max}, were identified [5]. The overall acetate uptake rate of *G. sulfurreducens* was calculated using the experimentally identified uptake parameters (Equation 11) [5, 78]. The V^{max} for acetate uptake of *R. ferrireducens* was calculated from regression analysis of batch growth data [20] and the K_s was assumed to be equal to the lowest acetate saturation constant value of *G. sulfurreducens* (Equation 12). The ATP maintenance requirement value for *G. sulfurreducens* and *R. ferrireducens* was set to 0.45 mmol ATP/gDW/hr [3, 4]. In the following equations, [S] represents the concentration of substrate S, and V_S^A represents the uptake rate of substrate S by organisms A.

$$V_{ac}^{Gs} = \frac{13.3[Acetate]}{[Acetate]+0.77} + \frac{2[Acetate]}{[Acetate]+0.167} + \frac{2.67[Acetate]}{[Acetate]+0.012} \quad (11)$$

$$V_{ac}^{Rf} = \frac{1.71[Acetate]}{[Acetate]+0.012} \quad (12)$$

Ammonium serves as a nitrogen source for *G. sulfurreducens* and *R. ferrireducens*, and it was assumed that maximum ammonium uptake rates were equal to the stoichiometric

ammonium requirements at their respective maximum growth rates, as calculated with FBA. The K_s for ammonium was assumed to be similar to that of *E. coli* [79].

$$V_{NH_4}^{Gs} = \frac{0.468[Ammonium]}{[Ammonium] + 0.074} \quad (13)$$

$$V_{NH_4}^{Rf} = \frac{0.127[Ammonium]}{[Ammonium] + 0.074} \quad (14)$$

4.3 Modeling Resource Availability

In anoxic sedimentary environments, complex organic matter is fermented with acetate as the primary fermentation product [9, 80, 81]. Thus, the slow steady release of acetate from fermentation is expected to be the primary natural source of acetate in the subsurface sediments at the Rifle site.

The rates of microbial processes have been studied in various organics-poor sediments. In a shallow sandy aquifer similar to the Rifle aquifer, the rate of acetate oxidation associated with iron-reduction, sulfate-reduction, and methanogenesis was reported to be between 0 – 0.5 uM/hr [82]. Similar values were reported for oligotrophic lake and marine sediments [83, 84]. The acetate turnover rate in a deep aquifer is measured to be 0.0135 μM/hr at 35m depth [85], which is assumed to be the lower bound for our simulations.

Based on these previous findings, we assumed the acetate flux into the subsurface at Rifle is between 0 to 0.54 μM/hr prior to the stimulation of metabolism with the addition of acetate. This value is consistent with the values reported by Hensen et al. (2001). Lovley and Klug (1986) have used 3 μM/hr as the acetate turnover rate in order to model the organics-poor sediment environment [86]. We assumed a lower value because iron reducers only use a portion of the acetate.

The Ammonium concentrations were set to range from 5 to 400 μM, which correspond to the ammonium concentrations previously observed at the Rifle site [16](Figure 1-2C).

Previous sediment sampling at bioremediation sites reported the Fe(III) concentration to be in the range of 5 - 40 μmol/g of sediment [7, 15, 87], which includes

both microbially reducible Fe(III) and Fe(III) that is resistant to reduction. If it is assumed that the sediment density is 2 g/ml [88] and that approximately 50% of Fe(III) is bioavailable, then 2.5 - 20 mmoles of Fe(III) per liter of groundwater is available for microbial reduction. Therefore, the initial Fe(III) concentration was assumed to be 10 mM for both pre-injection and during-injection simulations.

The initial cell concentration for both *G. sulfurreducens* and *R. ferrireducens* were assumed to be 10^5 cells/L based on previous results for the Rifle site [89]. The average cell mass of *G. sulfurreducens* is experimentally measured to be 10^{-12} g/cell (Appendix I). Assuming the physical densities of the intracellular content of the two organisms are the same, the *R. ferrireducens* cell mass was calculated to be 6.25 x 10^{-12}g/cell using the volume ratio between *G. sulfurreducens* and *R. ferrireducens*. Recent studies have demonstrated that high proportion of *Geobacter* species do not firmly attach to subsurface sediments at the Rifle site [90] and therefore it was assumed that cells were planktonic and that biomass was fully affected by dilution due to groundwater flow.

The injection of acetate to promote U(VI) reduction at the Rifle site results in acetate concentrations of 3-5 mM [7, 15]. The acetate injection rate was calculated by multiplying the acetate concentration of 3mM by the dilution rate, resulting in an acetate flux of 0.0042 mM/hr. This value was used to simulate the acetate flux during acetate injection. Since the measured ammonium concentrations *in situ* did not change during the course of bioremediation, the ammonium concentration during acetate amendment was fixed at 400 μM for the ammonium excess simulation, and fixed at 5 μM for the ammonium-limiting simulation.

The groundwater flow in the subsurface is modeled using a dilution rate of 0.034 day^{-1}, or 0.0014 hr^{-1}. This dilution rate is calculated by dividing the linear flow rate at Rifle (0.85 m/day) by the length of the experimental plot (24 m).

The simulation parameters are summarized in 0

4.4 Treatment of Experimental Data and Model Assessment

Data from the 2007 field experiment at Rifle Colorado [16] was used to assess the accuracy of the community dynamics predicted by the model. This data includes the initial and average ammonium concentrations as well as the in situ 16S rRNA measurement of *G. sulfurreducens* and *R. ferrireducens* abundance prior to the start of the acetate injection (day 0) and 9, 14, 18 days after the start of the injection (Figure 1-2C). In order to compare the relative abundance of *Geobacter* and *Rhodoferax* species mathematically, we defined a metric called "*Geobacter* fraction" (Equation 15). A higher *Geobacter* fraction value indicates a greater abundance of *Geobacter* species relative to *Rhodoferax*. The experimentally measured 16S rRNA abundance data was converted to *Geobacter* fraction value using equation Equation 15. Here, it is assumed that the number of 16s rRNA gene copies corresponding to a particular species is directly related to the number of organisms of this species.

$$Geobacter \text{ fraction} = \frac{\text{Number of } G.\,sulfurreducens}{\text{Number of } G.\,sulfurreducens + \text{Number of } R.\,ferrireducens} \qquad (15)$$

The prediction accuracy of the model was accessed for both natural conditions and during-injection conditions by comparing simulated *Geobacter* fractions with experimental *Geobacter* fractions at test-wells D02, D05, and D08. For both cases, the ammonium concentrations are set to the measured concentrations prior to acetate injection at these well.

4.5 Assumed Geometry

Our simulations assumed that the geometry of the uranium-contaminated subsurface environment to be a chemostat. This implied the assumption of spatial homogeneity, and greatly simplifies the transport and geochemical process. Because the focus of this thesis is on modeling the microbial community, not geochemistry and transport, this simplification was introduced.

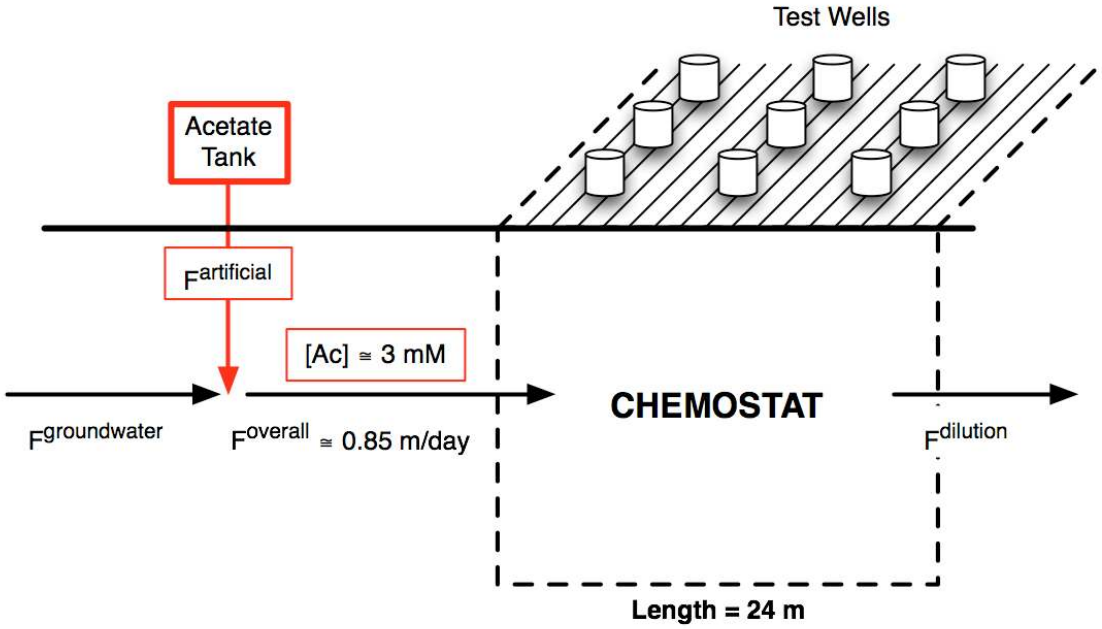

Figure 4-1. Assumed Geometry

This figure illustrates the assumed geometry of the simulations. Here, the parts of the figure shown in red are only present during acetate injection; the parts of the figure shown in black are present both prior to and during acetate injection.

During acetate injection, the artificial flow rate is very small, therefore has minimal effect on the overall flow rate. Therefore, the overall flow rate = the groundwater flow rate = the dilution flow rate. The linear flow rate is measured to be 0.85 m/day, and the length of the test plot is 24 m. The dilution rate is calculated to be 0.00141 hr^{-1}.

4.6 List of Assumptions

This section summarizes the assumptions made in our simulation.

1. Cells were assumed to be in internal steady state. This is the basic assumption of constraint-based metabolic modeling.
2. The relationship between substrate concentration and the upper limit of substrate uptake rates follow Michaelis-Menten relationship.
    a. Acetate uptake Ks of *Rhodoferax ferrireducens* is the same as *Geobacter sulfurreducens*, because they must compete for acetate in the same environment.
    b. Ammonium uptake Ks of both *Rhodoferax ferrireducens* and *Geobacter sulfurreducens* are the same as that of *Escherichia coli*.
3. Our simulations assumes that the geometry of the uranium-contaminated subsurface environment to be a chemostat. This implies the assumption of spatial homogeneity, as well as greatly simplifies the transport process.
4. The physical density (mass/volume) of the intracellular contents of *G. sulfurreducens* and *R. ferrireducens* are assumed to be the same. The average mass of *G. sulfurreducens* (g/cell) is measured experimentally. The average mass of *R. ferrireducens* is calculated based on volume ratio of the two cells. The volumes of the cells are calculated based on the published cell dimensions [18, 20]. Cells are assumed to be rod-shaped. (See Appendix I for details).

Chapter 5. RESULTS AND DISCUSSION

5.1 Community Competition Under Natural Conditions

Prior to the addition of acetate to the groundwater, fermentation of complex organic matter is expected to be the primary source of acetate to *Rhodoferax* and *Geobacter* species. The rate of this natural supply of acetate at the Rifle site is not known, but is expected to fall within the range of acetate turnover rates that have been observed in various sedimentary environments [82-86]. The steady state *Geobacter* fractions generated using low acetate turnover rates of 0.016, 0.027, and 0.04 μM/hr are compared with the *Geobacter* fraction values calculated from experimental measurement at day 0 (Figure 5-1). This comparison suggests that the acetate turnover rates is close to 0.27 μM/hr at well D02, is close to 0.016 μM/hr at well D05, and is close to 0.04 μM/hr at well D08 (Figure 5-1). All three inferred acetate turnover rates falls within the range measured in similar environments (Figure 5-1) [82], which supports the predicted competition dynamics at natural conditions. These results also suggest that the model could be used to predict the community dynamics under natural conditions more accurately if measurements of the acetate turnover rates at the three wells prior to injection were available.

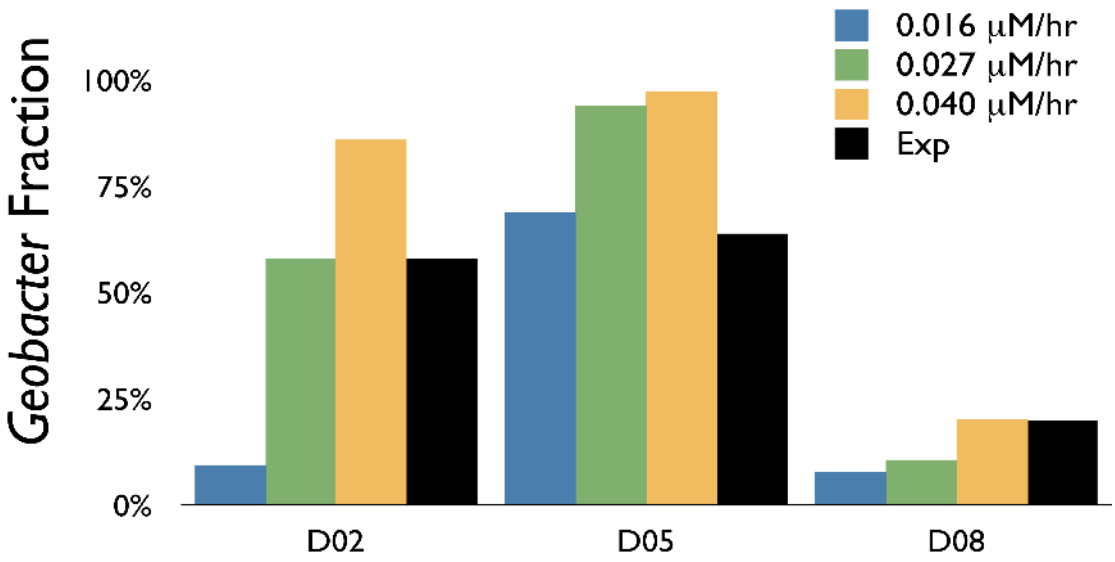

Figure 5-1. Comparison between simulated and measured *Geobacter* fraction under natural conditions

Predicted *Geobacter* fractions at D02, D05, and D08 prior to acetate addition are generated using acetate turnover rates of 0.016, 0.027 and 0.040 μM/hr. The predictions are compared with the *Geobacter* fraction values calculated from experimental 16S rRNA measurements at the respective wells, at day 0. This comparison suggests that the acetate turnover rates is close to 0.016 μM/hr at well D02, is close to 0.027 μM/hr at well D05, and is close to 0.040 μM/hr at well D08. All three inferred acetate turnover rates falls within the range measured in similar environments, which supports the predicted competition dynamics at natural conditions.

The community competition was simulated over three different (low, medium, high) acetate turnover ranges (Figure 5-2). The simulations suggested that at low acetate turnover rates *Rhodoferax* species are likely to be more abundant than *Geobacter* species, especially when ammonium is in excess. This prediction is consistent with the results of analysis of 16S rRNA gene sequences at the Rifle site prior to the addition of acetate [16].

Risso *et al.* analyzed the energetics of *R. ferrireducens* by comparing predicted yields with experimental yields under multiple conditions, and found that the proton translocation stoichiometry at cytochrome reductase of $2H^+/2e^-$ was consistent with the data for *R. ferrireducens* [4], whereas the stoichiometry at this step that could explain experimental data was found to be $1H^+/2e^-$ for *G. sulfurreducens* [3]. The doubling of cytochrome reductase energetic efficiency led to a significant increase in the efficiency of the electron transport chain and the predicted *Rhodoferax* biomass yield during Fe(III) respiration. FBA simulations show that under acetate-limited growth on Fe(III), the yield of *R. ferrireducens* is 0.0798 gDW/mmol of acetate, nearly two times the yield of *G. sulfurreducens* (0.0437 gDW/mmol of acetate). Thermodynamic analysis of cellular growth shows that the free energy of substrate oxidation can either be used to drive metabolic reactions at higher rates or to produce biomass; in other words, an organism can either optimize for substrate uptake rate or optimize for energetic efficiency [59, 60, 63, 91, 92]. Therefore, by choosing to optimize for efficiency, *Rhodoferax* has higher biomass yield at the expense of growth rate, resulting in a significantly lower substrate uptake rate compared to *Geobacter* exemplified by the observation that the maximum

acetate uptake rate of *G. sulfurreducens* (18 mmol/gDW/hr, equation 1) is more than ten fold higher than that of *R. ferrireducens* (1.71 mmol/gDW/hr, equation 2).

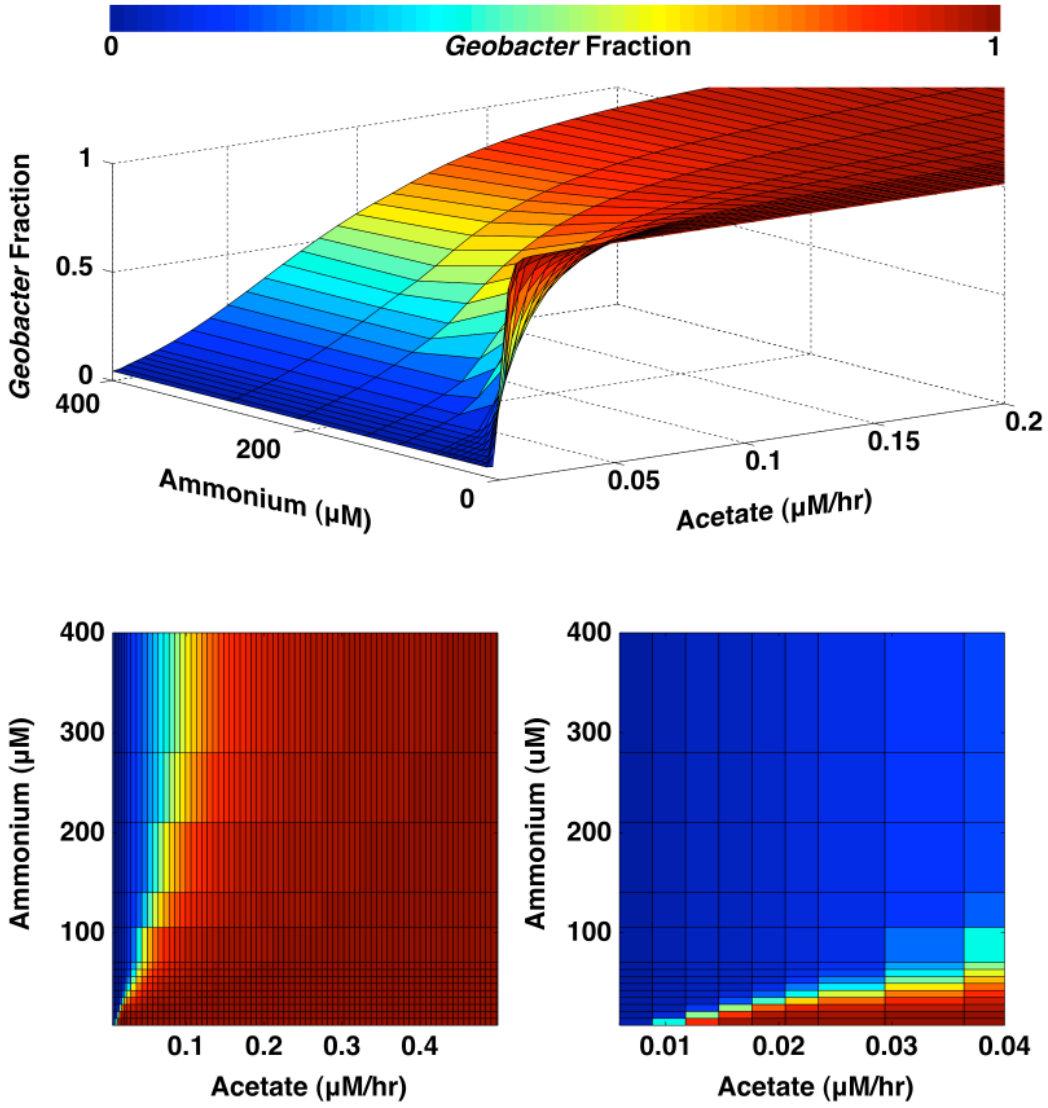

Figure 5-2. The relative success of *Geobacter* and *Rhodoferax* in Fe(III) reducing community prior to acetate amendment.

The steady state community compositions at three different acetate turnover rate ranges are simulated. *Geobacter* fraction is used to measure the relative success of *Geobacter* to *Rhodoferax* species. The competition with respect to ammonium concentration and acetate turnover rate is viewed at three different scales with respect to the acetate turnover rate. (A) Acetate turnover rates range from 0 to 0.2 μM/hr. At this scale, the nonlinearity of the competition is highlighted. (B) Acetate turnover rates range from 0 to 0.54 μM/hr, corresponding to the range of subsurface acetate availability reported by Hansen *et al.* (2001). (C). Acetate turnover rates range from 0 to 0.04 μM/hr, corresponding to the rates measured in an aquifer extremely poor in acetate (Chapelle and Lovley, 1990).

It was previously shown that yield-strategists are favored over rate-strategists under low substrate flux conditions [60]. The same rationale can be applied to the anoxic ferric microbial community. Growth rate is the product of substrate uptake rate and yield ($\mu = Vs \times Y$). At low acetate turnover conditions, the low environmental acetate flux limits the uptake rate of *Geobacter* to a fraction of its maximum. If both organisms have similar uptake rates, then the growth rate of *Rhodoferax* is significantly higher since its yield is twice that of *Geobacter*. This explains the abundance of *Rhodoferax* at low acetate turnover conditions when ammonium is readily available (Figure 5-2C). As acetate turnover rate increases, the acetate uptake limitation is relaxed. When the acetate turnover rate is sufficiently high to allow *Geobacter* uptake rates to become more than two times that of *Rhodoferax*, the growth rate of *Geobacter* becomes greater than that of *Rhodoferax*. Therefore, *Geobacter* becomes more competitive at higher acetate fluxes (Figure 5-2A, B).

The modeling suggests that the availability of ammonium in the sediments also plays a major role in the relative abundance under natural conditions in the sediments, with *Geobacter* favored at low ammonium conditions (Figure 5-1,Figure 5-2). The community composition varied non-linearly with respect to ammonium concentration and acetate turnover rate (Figure 1-2A). The region of co-existence (*Geobacter* fraction between 0.4 to 0.6) of *Rhodoferax* and *Geobacter* under steady-state conditions was narrow; minute changes in acetate and ammonium flux led to the complete dominance of one organism (Figure 5-2B, C). The simulations predicted that as the availability of ammonium

decreased, *Geobacter* became more competitive with *Rhodoferax* at low acetate turnover rates (Figure 5-2C). This can be attributed to the ability of *Geobacter* to fulfill its nitrogen requirements from fixation of nitrogen whereas *Rhodoferax* is incapable of nitrogen fixation. Availability of acetate in excess results in the limitation in ammonium for *Rhodoferax*, favoring the growth of *Geobacter*. High expression of genes for nitrogen fixation in *Geobacter* species living in a diversity of subsurface sediments [89, 93, 94] has suggested that they are actively involved in nitrogen fixation in the subsurface. *Geobacter* nitrogen fixation genes may even be expressed when low (< 50 μM) concentrations are available in sediments [95], suggesting that such subsurface sediments may well contain microzones that are ammonium-depleted. The presence of such microzones would further facilitate co-existence of *Geobacter* and *Rhodoferax* with growth of *Geobacter* favored in the ammonium-depleted microzones. However, the current model does not incorporate spatial heterogeneity and therefore, cannot predict such spatial variations in community composition.

5.2 Community Competition when Acetate is added to the Subsurface

Our simulation predictions of the community composition at test wells D02, D05, and D08 during acetate addition shows the same trend as the values calculated from 16S rRNA measurements (Figure 5-3). These simulations (Figure 5-3) agree with previous observations that the addition of millimolar concentrations of acetate to the subsurface in order to stimulate in situ uranium bioremediation at the Rifle site significantly influences the relative proportions of *Geobacter* and *Rhodoferax*, with *Geobacter* species consistently becoming the predominant microorganisms regardless of ammonium availability [7, 15, 16, 89]. Furthermore, the predicted number of *Geobacter* cells agrees in order of magnitude with the measured number of *Geobacter* cells at day 19 (Figure 5-4).

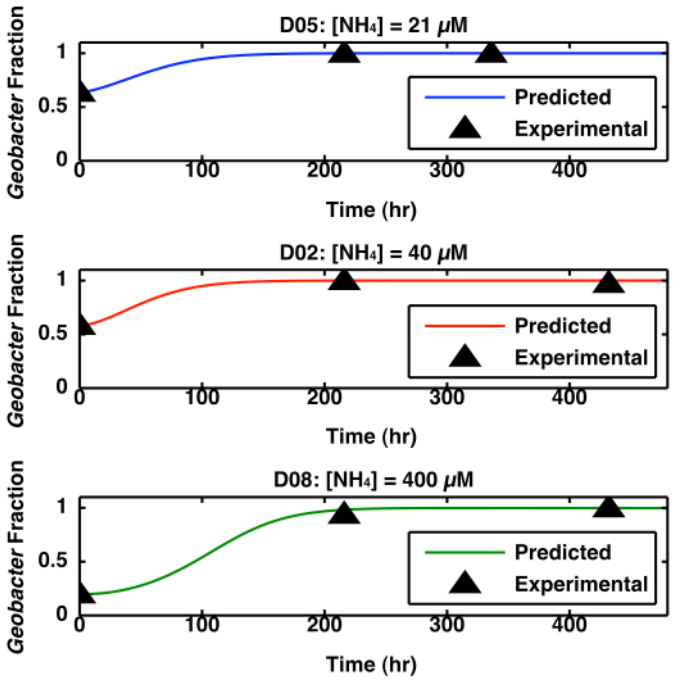

Figure 5-3. Comparison between predicted and measured *Geobacter* fractions during acetate addition.

The predicted *Geobacter* fractions of wells D05, D02, and D08 are compared with the experimentally measured fractions at the respective wells. Simulations are initiated with the *Geobacter* fractions and ammonium concentrations measured at Day 0 in wells D05 (64%, 21 μM), D02 (58%, 40μM), and D08 (20%, 400μM). The predicted *Geobacter* fractions (solid lines) are compared with the *Geobacter* fractions calculated from experimentally 16S rRNA measurements (▲).

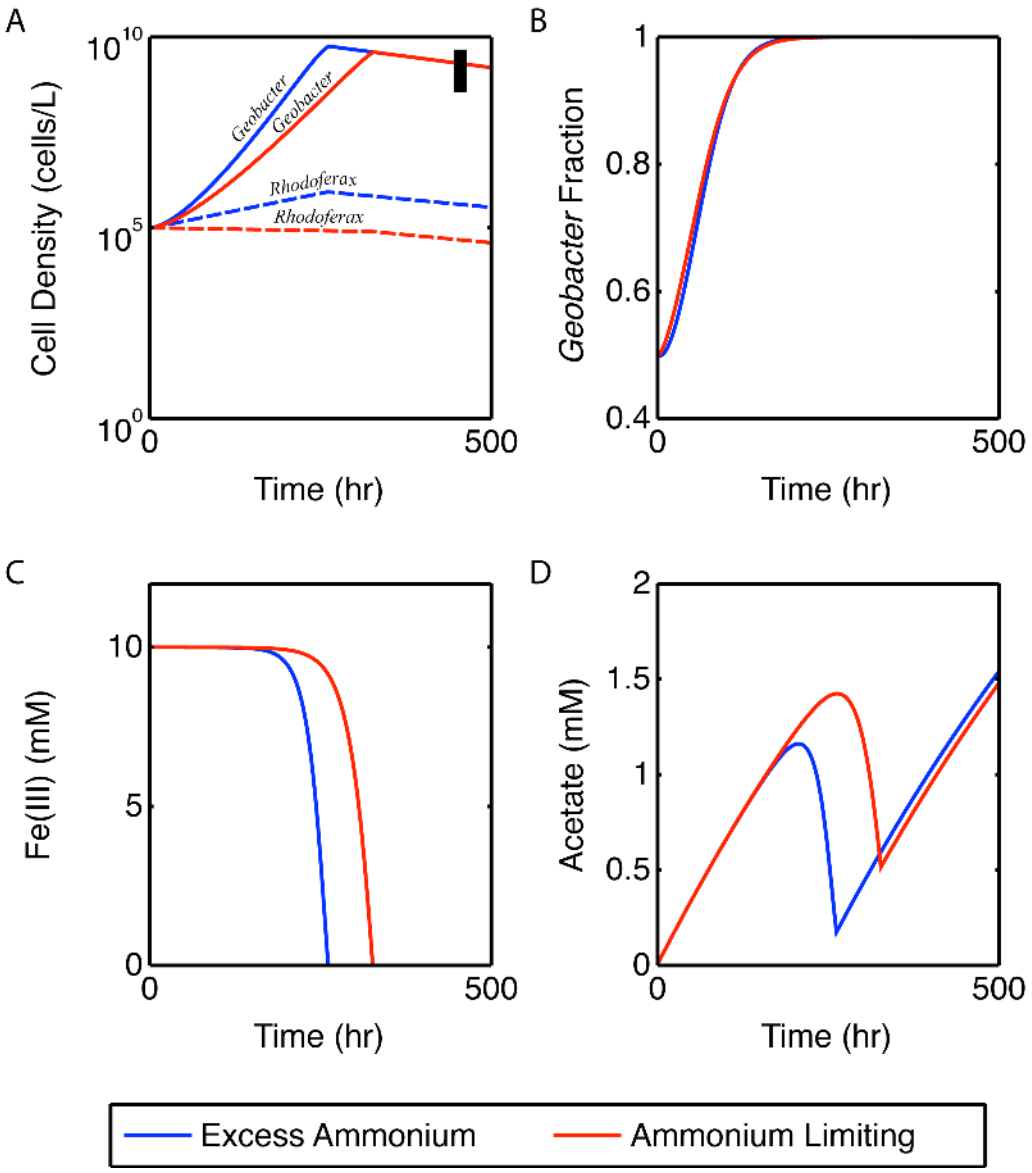

Figure 5-4. Simulation of the competition dynamics in a Fe(III) reducing community during acetate addition.

Biomass concentrations of *G. sulfurreducens* and *R. ferrireducens* (A), *Geobacter* fractions (B), acetate concentration (C), and Fe(III) concentration (D) under both ammonium-limiting and ammonium excess conditions are shown. *Geobacter* out-competes *Rhodoferax* soon after acetate addition begins under both conditions. The black bar in panel A represents the measured range of *Geobacter* cell concentration at day 19 [89].

Simulations are initialized with equal numbers of *Geobacter* and *Rhodoferax*. Acetate injection rate of 3mM/day (4.2 µM/hr) is used for both ammonium-limiting ([ammonium] = 0.005 mM) and ammonium excess conditions ([ammonium] = 0.4 mM).

Note: The Y-axis of panel A is in log scale, where as the Y-axis of panels B,C,D are in linear scale.

The reasons for this were readily apparent from the dynamic genome-scale modeling (Figure 5-3). Here, the acetate flux was assumed to be 4.2 μM/hr. At this acetate flux, the ammonium turnover rate in the ammonium excess case is more than sufficient for biomass synthesis and is not limiting. (The ammonium turnover rate is estimated by multiplying the dilution rate and the steady ammonium concentration to be 0.56 μM/hr, Appendix I) Whereas in the ammonium limiting case, the ammonium flux (0.035 μM/hr) is the primary limitation for growth at the same level of acetate availability. *Geobacter* rapidly responded to increased acetate availability with a substantial increase in biomass, whether or not sufficient ammonium was available to completely support all of the acetate-dependent growth (Figure 5-4A,B). In contrast, the growth rate of *R. ferrireducens* was just above the dilution rate in the ammonium excess case, whereas there is a loss in *Rhodoferax* biomass in the ammonium limiting case. This reflects the absolute requirement (Figure 5-4A,B) of *Rhodoferax* for ammonium to support growth. Low ammonium delayed, but did not prevent extensive growth of *Geobacter*. However, the maximum amount of *Geobacter* biomass was lower under ammonium-limiting conditions due to the increased energetic demands for nitrogen fixation (Figure 5-4A). With extended time Fe(III) was depleted and *Geobacter* declined (Figure 5-4A,C). Acetate was never exhausted during the simulation (Figure 5-4D); however, if more Fe(III) was made available, acetate was completely consumed before the complete utilization of Fe(III) (data not shown).

The high flux of acetate from the artificial addition allows both species to achieve their maximum acetate uptake rate. Since the maximum acetate uptake rate of *Geobacter* is more than ten times higher than that of *Rhodoferax*, whereas the yield of *Rhodoferax* is

only twice higher than that of *Geobacter*, the growth rate of *Geobacter* is significantly higher than that of *Rhodoferax* when both organisms utilize acetate at their respective maximum uptake rates. Therefore, during bioremediation, *Geobacter*'s advantage in uptake rate outweighs *Rhodoferax*'s advantage in yield, leading to the overwhelming success of *Geobacter.*

The cell densities and Fe(III) concentration prior to acetate injection can vary greatly prior to acetate amendment. In order to evaluate the sensitivity of the competition dynamics to variations in the initial cell densities, and Fe(III) concentrations, simulations with different initial Fe(III) concentrations (2.5, 5, 10, and 20 mM) and cell densities (10^4, 10^5, and 10^6 cells/L) were performed. These simulations showed no significant changes in the dynamics of the competition, suggesting that the variations in these two parameters will not affect the increase in the *Geobacter* fraction during *in situ* bioremediation.

5.3 Predicted changes in metabolic states-bioremediation implications

An additional feature of the genome scale metabolic models is their capability to predict changes in the metabolic states of microorganisms under different environmental conditions. The model predicted three metabolic phases for each organism: the acetate-limiting growth phase; the ammonium-depleted phase and the Fe(III)-depleted death phase;. Under ammonium-depleted conditions, *R. ferrireducens* is predicted to experience a maintenance phase with no associated growth because of the lack of ammonium, but with the ability to generate ATP by oxidizing acetate coupled to Fe(III) reduction. In contrast, *G. sulfurreducens* is able to grow in the absence of ammonium by nitrogen fixation.

The necessity for nitrogen fixation is predicted to have a number of environmentally relevant physiological consequences for *Geobacter* (Figure 5-5). The genome-scale model predicts that in order to meet increased energetic demands associated with nitrogen fixation more acetate enters the TCA cycle and there are higher fluxes through NADH dehydrogenase and extracellular electron transfer, and ATP synthase (Figure 5-5). Under nitrogen-fixing conditions, less biomass is produced which is reflected in less acetate flux through acetate kinase, as well as less pyruvate production through pyruvate oxidoreductase for biomass synthesis. These changes in metabolic fluxes are predicted to result in ca. 30% reduction in growth yield (Figure 5-5). A reduction of *Geobacter* biomass yield under nitrogen-fixation conditions have been observed experimentally [96].

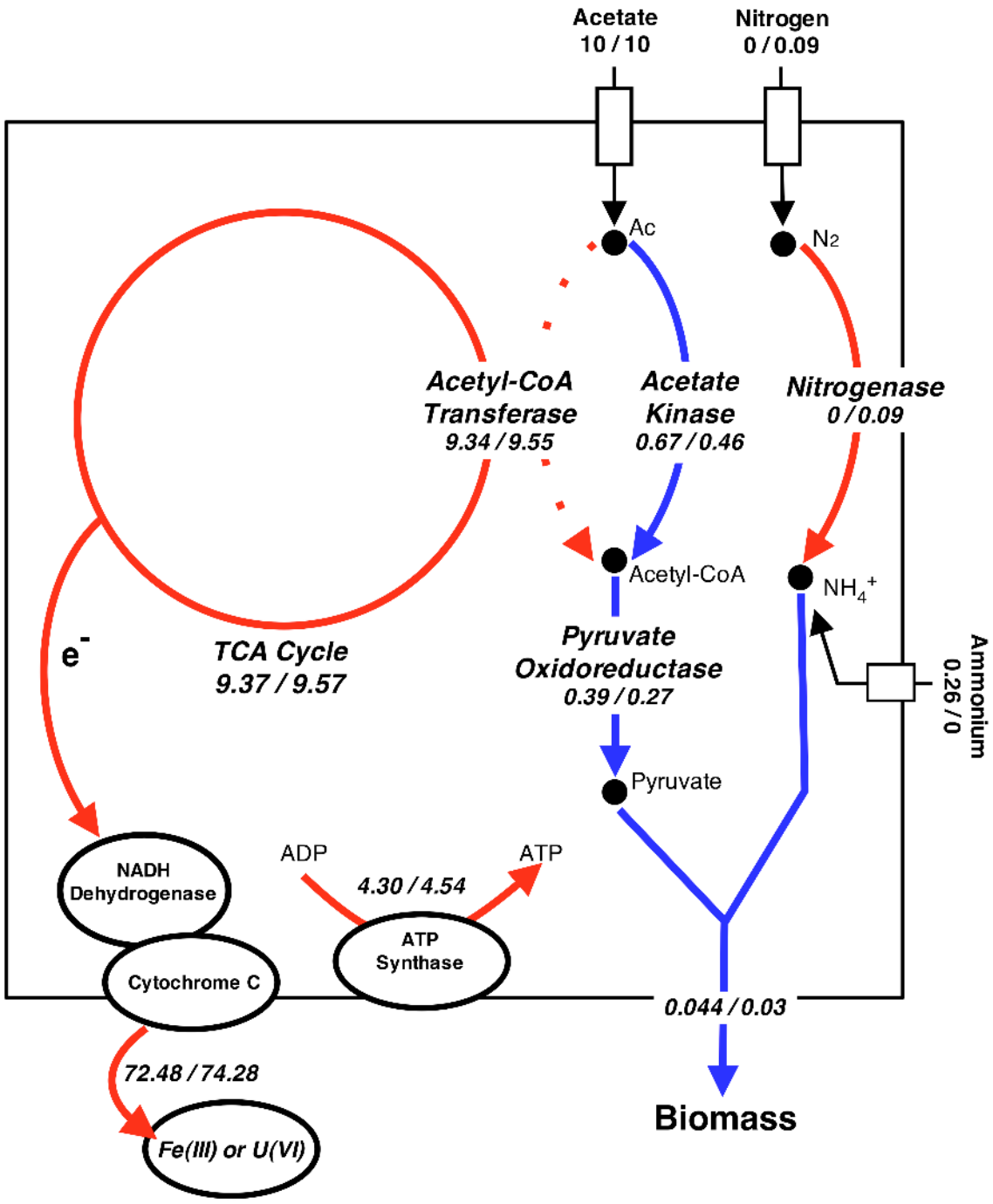

Figure 5-5. Comparison of the predicted flux distribution of *G. sulfurreducens* during growth with ammonium vs. nitrogen-fixation dependent growth

The predicted flux distributions of *G. sulfurreducens* during growth with unlimited ammonium uptake and nitrogen-fixation dependent growth are compared. The biomass flux is measured in hr^{-1}, all other fluxes are measured in mmol gDW^{-1} hr^{-1}. Red fluxes are increased during nitrogen fixation, blue fluxes are decreased during nitrogen fixation. The first number represents the flux through the reaction when ammonium is acquired through environmental uptake; the second number represents the flux through the reaction when ammonium is provided through nitrogen-fixation.

The predicted shift in metabolism associated with nitrogen fixation could have a significant impact on the effectiveness of *in situ* uranium bioremediation. The rate of U(VI) reduction depends on both the specific uranium reduction rate and biomass concentration. During nitrogen fixation, the rate of U(VI) reduction per cell may increase due to the up-regulation of respiration, at the expense of biomass production. This prediction of the model is consistent with field results at the Rifle site. In the 2007 field experiment, U(VI) was much more effectively removed from the groundwater at sites low in ammonium than at a site with relatively high ammonium concentrations [16]. It may be possible with dynamic optimization techniques to predict from genome-scale metabolic models, the optimal ammonium concentrations for maximal rates of U(VI) reduction. This would be analogous to recent design of a *G. sulfurreducens* strain with increased respiration rates and lower biomass yields via genome-scale metabolic modeling [33].

Chapter 6. Conclusion

6.1 Implications of the *Geobacter* and *Rhodoferax* community simulations

The simulations suggest that *Geobacter* and *Rhodoferax* species have adopted very different strategies for growth in subsurface environments. *Geobacter* have sacrificed maximizing yield from substrate utilization in favor of the capability of rapid growth and the ability to grow in the absence of ammonium whereas *Rhodoferax* are more optimized for higher growth yields. Both strategies appear to be adaptive for growth under natural subsurface conditions at the Rifle site. *Geobacter* and *Rhodoferax* are found within the same sampling zones. This probably reflects growth of *Geobacter* and *Rhodoferax* species in different microenvironments within the heterogeneous subsurface environment. The ability of *Geobacter* to grow faster than *Rhodoferax* at high acetate concentrations and to multiply in the absence of ammonium permits it to rapidly respond to the artificial conditions imposed when acetate is added to promote *in situ* uranium bioremediation. It is fortuitous that *Geobacter* outcompete *Rhodoferax* under these conditions, because pure culture studies have suggested that *Geobacter* [18], but not *Rhodoferax* [20] species are capable of U(VI) reduction. If this distinction were true for all *Rhodoferax* species then *in situ* uranium reduction would be much less effective if *Rhodoferax* could readily compete with *Geobacter* under high acetate/low ammonium conditions.

There are other microbial interactions that are likely to impact on the effectiveness of *in situ* uranium bioremediation. Most notably, the consumption of added acetate by acetate-oxidizing sulfate reducers that are ineffective in U(VI) reduction (Anderson *et al.* 2003) may limit U(VI) reduction by *Geobacter* species, decreasing the efficacy of the

bioremediation [7, 15]. As genome-scale models for these sulfate reducers become available it should be possible to evaluate this interaction in a manner similar to that reported here for *Geobacter*/*Rhodoferax* interactions. Furthermore, the increasing availability of the genome sequences of environmentally relevant microorganisms should make it feasible to apply genome-scale metabolic modeling to further investigate the ecology of a wide diversity of microbial ecosystems.

6.2 Thesis Objectives Achieved

In section 1.5, we have outlined the objectives of this thesis as:

1. To develop a **general** *computational framework* applicable to complex (dynamic, multi-species) microbial communities.
2. To apply this *computational framework* to the investigation of the *Geobacter* and *Rhodoferax* microbial community in uranium-contaminated subsurface. In particular, we aim to answer the following two questions:
    a. Why do two acetate-oxidizing iron-reducing organisms occupy the same niche?
    b. Will the existence of *Rhodoferax* species affect the outcome of uranium bioremediation?

We have achieved both of these objectives:

1. We have developed the Dynamic Multi-species Metabolic Modeling (DMMM) framework. The DMMM framework has proved to be a **general** *computational framework* applicable to complex (dynamic, multi-species) microbial communities. To date, the framework has been applied to multiple microbial communities, one of which is the *Geobacter* and *Rhodoferax* microbial community discussed in this thesis. The DMMM model has proved to be very efficient to use – for example, after the establishment of the standard protocols, the development of the *Geobacter*, *Desulfovibrio vulgaris*, and acetate-oxidizing

sulfate reducers took about one week time to complete. See Appendix III for a list of the microbial communities modeled using DMMM.

2. Using the DMMM framework, we investigated the dynamics of the *Geobacter* and *Rhodoferax* community in uranium-contaminated subsurface prior and during acetate addition. Our investigations have yielded answers to the two initial motivating questions:

    a. Why do two acetate-oxidizing iron-reducing organisms occupy the same niche?

        The community composition is highly sensitive to acetate and ammonium availability. Prior to acetate injection, the abundance of these two metabolites varies temporally and spatially within the subsurface environment, thus conditionally favoring either *Geobacter* or *Rhodoferax* species. This allows these two iron-reducing organisms to simultaneously occupy the same niche.

    b. Will the existence of *Rhodoferax* species affect the outcome of uranium bioremediation?

        During acetate addition, the high acetate flux strongly favors *Geobacter* species, the rate-strategist. In all simulations of the acetate addition phase, *Geobacter* completely dominates the community. Therefore, the existence of *Rhodoferax* species does not affect the outcome of uranium bioremediation.

6.3 Future Recommendations

1. To fully understand the uranium-contaminated subsurface environment, the DMMM model should be coupled with the reactive transport model, in similar fashion as the model presented by Scheibe *et al.*[23].
2. The DMMM framework should be used as an *in silico* tool to test-out novel bioremediation strategies, such as lactate addition, prior to incurring the cost of *in situ* experiments.
3. One significant hurdle in the development of the *Geobacter* and *Rhodoferax* model was the difficulty in acquiring **high-quality** experimental data. Entering low-quality data into a complex metabolic model such as the DMMM is the scientific equivalent of making a high-end sports car run on dry grass. Hopefully the work presented in this thesis will help to bridge the gap between experimentalists and modelers.
4. This thesis investigates the competition between a rate-strategist and a yield-strategist at the ecological level. However, while the rate vs. yield tradeoff is well understood at the chemical reaction level, less is known about the specific mechanism this tradeoff is reflected in the cell metabolism. Investigation into the evolution and design of the electron transport chain should provide insights to this problem.

Bibliography

1. Zhuang K, Izallalen M, Mouser P, Richter H, Risso C, Mahadevan R, Lovley DR: **Genome-Scale Dynamic Modeling of the Competition Between *Rhodoferax* and *Geobacter* in Anoxic Subsurface Environments**. *ISME J* Submitted.
2. Zhuang K, Zhao J, Mahadevan R: **Constraint-Based Metabolic Model: an Interdisciplinary Tool for Improving Biotechnology Applications**. *Journal of Royal Society Interface* Submitted.
3. Mahadevan R, Bond DR, Butler JE, Esteve-Nunez A, Coppi MV, Palsson BO, Schilling CH, Lovley DR: **Characterization of metabolism in the Fe(III)-reducing organism *Geobacter sulfurreducens* by constraint-based modeling.** *Appl Environ Microbiol* 2006, **72**(2):1558-1568.
4. Risso C, Sun J, Zhuang K, Mahadevan R, DeBoy R, Ismael W, Bui O, Schilling CH, Lovley DR, Methe BA: **Genome scale comparisons and constraint-based metabolic reconstructions of the facultative anaerobic Fe(III)-reducer *Rhodoferax ferrireducens***. Submitted.
5. Richter H, Risso C, Lovley DR: **Evidence for multiple acetate carriers in *Geobacter sulfurreducens***. *Microbiology* Submitted.
6. DOE U: **NABIR Report**. In.; 2003.
7. Anderson RT, Vrionis HA, Ortiz-Bernad I, Resch CT, Long PE, Dayvault R, Karp K, Marutzky S, Metzler DR, Peacock A *et al*: **Stimulating the in situ activity of *Geobacter* species to remove uranium from the groundwater of a uranium-contaminated aquifer.** *Appl Environ Microbiol* 2003, **69**(10):5884-5891.
8. Lovley DR: **Dissimilatory Fe(III)- and Mn(IV)-Reducing Prokaryotes**. In: *The prokaryotes*. Edited by Dworkin M, Falkow S, Rosenberg E, Schleifer KH, 3rd edn. New York: Springer; 2006: liii, 1143 p.
9. Lovley DR, Holmes DE, Nevin KP: **Dissimilatory Fe(III) and Mn(IV) reduction**. *Adv Microb Physiol* 2004, **49**:219-286.
10. Lovley DR: **Dissimilatory Fe(III) and Mn(IV) reduction**. *Microbiol Rev* 1991, **55**(2):259-287.
11. Lovley DR: **Bioremediation. Anaerobes to the rescue**. *Science* 2001, **293**(5534):1444-1446.
12. Lovley DR, Phillips EJ: **Reduction of uranium by Desulfovibrio desulfuricans**. *Appl Environ Microbiol* 1992, **58**(3):850-856.
13. Lovley DR, Phillips EJ, Caccavo F, Jr.: **Acetate oxidation by dissimilatory Fe(III) reducers**. *Appl Environ Microbiol* 1992, **58**(9):3205-3208.
14. Wall JD, Krumholz LR: **Uranium reduction**. *Annu Rev Microbiol* 2006, **60**:149-166.
15. Vrionis HA, Anderson RT, Ortiz-Bernad I, O'Neill KR, Resch CT, Peacock AD, Dayvault R, White DC, Long PE, Lovley DR: **Microbiological and geochemical**

heterogeneity in an in situ uranium bioremediation field site. *Appl Environ Microbiol* 2005, **71**(10):6308-6318.

16. Mouser PJ, N'Guessan AL, Elifantz H, Holmes DE, Williams KH, Wilkins MJ, Long PE, Lovley DR: **Influence of Heterogeneous Ammonium Availability on Bacterial Community Structure and the Expression of Nitrogen Fixation and Ammonium Transporter Genes during in Situ Bioremediation of Uranium-Contaminated Groundwater.** *Environmental Science & Technology* In Press.
17. Chang YJ, Long PE, Geyer R, Peacock AD, Resch CT, Sublette K, Pfiffner S, Smithgall A, Anderson RT, Vrionis HA *et al*: **Microbial incorporation of 13C-labeled acetate at the field scale: detection of microbes responsible for reduction of U(VI)**. *Environ Sci Technol* 2005, **39**(23):9039-9048.
18. Caccavo F, Jr., Lonergan DJ, Lovley DR, Davis M, Stolz JF, McInerney MJ: ***Geobacter sulfurreducens* sp. nov., a hydrogen- and acetate-oxidizing dissimilatory metal-reducing microorganism**. *Appl Environ Microbiol* 1994, **60**(10):3752-3759.
19. Lovley DR: **Dissimilatory metal reduction**. *Annu Rev Microbiol* 1993, **47**:263-290.
20. Finneran KT, Johnsen CV, Lovley DR: ***Rhodoferax ferrireducens* sp. nov., a psychrotolerant, facultatively anaerobic bacterium that oxidizes acetate with the reduction of Fe(III)**. *Int J Syst Evol Microbiol* 2003, **53**(Pt 3):669-673.
21. Rittmann BE, McCarty PL: **Environmental biotechnology : principles and applications**. Boston: McGraw-Hill; 2001.
22. Lovley DR: **Cleaning up with genomics: applying molecular biology to bioremediation**. *Nat Rev Microbiol* 2003, **1**(1):35-44.
23. Scheibe TD, Mahadevan R, Fang Y, Garg S, Long PE, Lovley DR: **Coupling a genome-scale metabolic model with a reactive transport model to describe in situ uranium bioremediation**. *Microbial Biotechnology* 2009, **2**(2):274-286.
24. Ibarra RU, Edwards JS, Palsson BO: ***Escherichia coli* K-12 undergoes adaptive evolution to achieve in silico predicted optimal growth**. *Nature* 2002, **420**(6912):186-189.
25. Reed JL, Palsson BO: **Thirteen years of building constraint-based in silico models of *Escherichia coli***. *J Bacteriol* 2003, **185**(9):2692-2699.
26. Reed JL, Vo TD, Schilling CH, Palsson BO: **An expanded genome-scale model of *Escherichia coli* K-12 (iJR904 GSM/GPR)**. *Genome Biol* 2003, **4**(9):R54.
27. Feist AM, Henry CS, Reed JL, Krummenacker M, Joyce AR, Karp PD, Broadbelt LJ, Hatzimanikatis V, Palsson BO: **A genome-scale metabolic reconstruction for *Escherichia coli* K-12 MG1655 that accounts for 1260 ORFs and thermodynamic information**. *Mol Syst Biol* 2007, **3**:121.
28. Feist AM, Palsson BO: **The growing scope of applications of genome-scale metabolic reconstructions using *Escherichia coli***. *Nat Biotechnol* 2008, **26**(6):659-667.
29. Segura D, Mahadevan R, Juarez K, Lovley DR: **Computational and experimental analysis of redundancy in the central metabolism of *Geobacter sulfurreducens***. *PLoS Comput Biol* 2008, **4**(2):e36.
30. Anesiadis N, Cluett WR, Mahadevan R: **Dynamic metabolic engineering for increasing bioprocess productivity**. *Metab Eng* 2008, **10**(5):255-266.

31. Burgard AP, Pharkya P, Maranas CD: **Optknock: a bilevel programming framework for identifying gene knockout strategies for microbial strain optimization**. *Biotechnol Bioeng* 2003, **84**(6):647-657.
32. Hjersted JL, Henson MA, Mahadevan R: **Genome-scale analysis of *Saccharomyces cerevisiae* metabolism and ethanol production in fed-batch culture**. *Biotechnol Bioeng* 2007, **97**(5):1190-1204.
33. Izallalen M, Mahadevan R, Burgard A, Postier B, Didonato R, Jr., Sun J, Schilling CH, Lovley DR: ***Geobacter sulfurreducens* strain engineered for increased rates of respiration**. *Metab Eng* 2008, **10**(5):267-275.
34. Pharkya P, Burgard AP, Maranas CD: **Exploring the overproduction of amino acids using the bilevel optimization framework OptKnock**. *Biotechnol Bioeng* 2003, **84**(7):887-899.
35. Pharkya P, Maranas CD: **An optimization framework for identifying reaction activation/inhibition or elimination candidates for overproduction in microbial systems**. *Metab Eng* 2006, **8**(1):1-13.
36. Methe BA, Nelson KE, Eisen JA, Paulsen IT, Nelson W, Heidelberg JF, Wu D, Wu M, Ward N, Beanan MJ *et al*: **Genome of *Geobacter sulfurreducens*: metal reduction in subsurface environments**. *Science* 2003, **302**(5652):1967-1969.
37. Sun J, Sayyar B, Butler JE, Pharkya P, Fahland TR, Famili I, Schilling CH, Lovley DR, Mahadevan R: **Genome-scale constraint-based modeling of *Geobacter metallireducens***. *BMC Syst Biol* 2009, **3**:15.
38. Barabasi AL, Oltvai ZN: **Network biology: understanding the cell's functional organization**. *Nat Rev Genet* 2004, **5**(2):101-113.
39. Clauset A, Moore C, Newman ME: **Hierarchical structure and the prediction of missing links in networks**. *Nature* 2008, **453**(7191):98-101.
40. Feist AM, Herrgard MJ, Thiele I, Reed JL, Palsson BO: **Reconstruction of biochemical networks in microorganisms**. *Nat Rev Microbiol* 2009, **7**(2):129-143.
41. Mahadevan R, Lovley DR: **The degree of redundancy in metabolic genes is linked to mode of metabolism**. *Biophys J* 2008, **94**(4):1216-1220.
42. Palsson B: **Systems biology : properties of reconstructed networks**. Cambridge ; New York: Cambridge University Press; 2006.
43. Price ND, Reed JL, Palsson BO: **Genome-scale models of microbial cells: evaluating the consequences of constraints**. *Nat Rev Microbiol* 2004, **2**(11):886-897.
44. DeJongh M, Formsma K, Boillot P, Gould J, Rycenga M, Best A: **Toward the automated generation of genome-scale metabolic networks in the SEED**. *BMC Bioinformatics* 2007, **8**:139.
45. **Available predictive genome-scale metabolic network reconstructions** [http://gcrg.ucsd.edu/In_Silico_Organisms/Other_Organisms]
46. Forster J, Famili I, Fu P, Palsson BO, Nielsen J: **Genome-scale reconstruction of the Saccharomyces cerevisiae metabolic network**. *Genome Res* 2003, **13**(2):244-253.
47. Mahadevan R: *Nat Rev Microbiol* Submitted.
48. Islam A: **Genome-scale metabolic model of *Dehalococcoides* sp. .** In.; Personal Communication.

49. Mahadevan R, Schilling CH: **The effects of alternate optimal solutions in constraint-based- genome-scale metabolic models**. *Metab Eng* 2003, **5**:264-276.
50. Mahadevan R, Edwards JS, Doyle FJ, 3rd: **Dynamic flux balance analysis of diauxic growth in *Escherichia coli***. *Biophys J* 2002, **83**(3):1331-1340.
51. Yang L, Mahadevan R, Cluett W: **A bilevel optimization algorithm to identify enzymatic capacity constraints in metabolic networks**. *Computers and Chemical Engineering* 2008, **32**:2072–2085.
52. Henry CS, Broadbelt LJ, Hatzimanikatis V: **Thermodynamics-based metabolic flux analysis**. *Biophys J* 2007, **92**(5):1792-1805.
53. Edwards JS, Ibarra RU, Palsson BO: **In silico predictions of *Escherichia coli* metabolic capabilities are consistent with experimental data**. *Nat Biotechnol* 2001, **19**(2):125-130.
54. Covert MW, Knight EM, Reed JL, Herrgard MJ, Palsson BO: **Integrating high-throughput and computational data elucidates bacterial networks**. *Nature* 2004, **429**(6987):92-96.
55. Covert MW, Xiao N, Chen TJ, Karr JR: **Integrating metabolic, transcriptional regulatory and signal transduction models in Escherichia coli**. *Bioinformatics* 2008, **24**(18):2044-2050.
56. Segre D, Vitkup D, Church GM: **Analysis of optimality in natural and perturbed metabolic networks**. *Proc Natl Acad Sci U S A* 2002, **99**(23):15112-15117.
57. Shlomi T, Berkman O, Ruppin E: **Regulatory on/off minimization of metabolic flux changes after genetic perturbations**. *Proc Natl Acad Sci U S A* 2005, **102**(21):7695-7700.
58. Fong SS, Burgard AP, Herring CD, Knight EM, Blattner FR, Maranas CD, Palsson BO: **In silico design and adaptive evolution of Escherichia coli for production of lactic acid**. *Biotechnol Bioeng* 2005, **91**(5):643-648.
59. Schuster S, Pfeiffer T, Fell DA: **Is maximization of molar yield in metabolic networks favoured by evolution?** *J Theor Biol* 2008, **252**(3):497-504.
60. Pfeiffer T, Schuster S, Bonhoeffer S: **Cooperation and competition in the evolution of ATP-producing pathways**. *Science* 2001, **292**(5516):504-507.
61. Novak M, Pfeiffer T, Lenski RE, Sauer U, Bonhoeffer S: **Experimental tests for an evolutionary trade-off between growth rate and yield in E. coli.** *Am Nat* 2006, **168**:242-251.
62. Beg QK, Vazquez A, Ernst J, de Menezes MA, Bar-Joseph Z, Barabasi AL, Oltvai ZN: **Intracellular crowding defines the mode and sequence of substrate uptake by Escherichia coli and constrains its metabolic activity**. *Proc Natl Acad Sci U S A* 2007, **104**(31):12663-12668.
63. Pfeiffer T, Bonhoeffer S: **Evolution of cross-feeding in microbial populations**. *Am Nat* 2004, **163**(6):E126-135.
64. Maharjan RP, Seeto S, Ferenci T: **Divergence and redundancy of transport and metabolic rate-yield strategies in a single Escherichia coli population**. *J Bacteriol* 2007, **189**(6):2350-2358.
65. Klamt S, Stelling J: **Two approaches for metabolic pathway analysis?** *Trends Biotechnol* 2003, **21**(2):64-69.

66. Stelling J, Klamt S, Bettenbrock K, Schuster S, Gilles ED: **Metabolic network structure determines key aspects of functionality and regulation**. *Nature* 2002, **420**(6912):190-193.
67. Braunstein A, Mulet R, Pagnani A: **Estimating the size of the solution space of metabolic networks**. *BMC Bioinformatics* 2008, **9**:240.
68. Price ND, Schellenberger J, Palsson BO: **Uniform sampling of steady-state flux spaces: means to design experiments and to interpret enzymopathies**. *Biophys J* 2004, **87**(4):2172-2186.
69. Thiele I, Price ND, Vo TD, Palsson BO: **Candidate metabolic network states in human mitochondria. Impact of diabetes, ischemia, and diet**. *J Biol Chem* 2005, **280**(12):11683-11695.
70. Tajima K, Aminov RI, Nagamine T, Matsui H, Nakamura M, Benno Y: **Diet-dependent shifts in the bacterial population of the rumen revealed with real-time PCR.** *Appl Environ Microbiol* 2001, **67**(6):2766-2774.
71. Konopka A: **Microbial Ecology: Searching for Principles**. *Microbe* 2006, **1**:175-179.
72. Vallino JJ: **Modeling microbial consortiums as distributed metabolic networks**. *Biol Bull* 2003, **204**(2):174-179.
73. Stolyar S, Van Dien S, Hillesland KL, Pinel N, Lie TJ, Leigh JA, Stahl DA: **Metabolic modeling of a mutualistic microbial community**. *Mol Syst Biol* 2007, **3**:92.
74. VanBriesen JM: **Evaluation of methods to predict bacterial yield using thermodynamics**. *Biodegradation* 2002, **13**(3):171-190.
75. Becker SA, Feist AM, Mo ML, Hannum G, Palsson BO, Herrgard MJ: **Quantitative prediction of cellular metabolism with constraint-based models: the COBRA Toolbox**. *Nat Protoc* 2007, **2**(3):727-738.
76. Varma A, Palsson BO: **Stoichiometric flux balance models quantitatively predict growth and metabolic by-product secretion in wild-type *Escherichia coli* W3110**. *Appl Environ Microbiol* 1994, **60**(10):3724-3731.
77. Varma A, Palsson BO: **Parametric sensitivity of stoichiometric flux balance models applied to wild-type *Escherichia coli* metabolism**. *Biotechnol Bioeng* 1995, **45**(1):69-79.
78. Esteve-Nunez A, Rothermich M, Sharma M, Lovley D: **Growth of *Geobacter sulfurreducens* under nutrient-limiting conditions in continuous culture**. *Environ Microbiol* 2005, **7**(5):641-648.
79. Reay DS, Nedwell DB, Priddle J, Ellis-Evans JC: **Temperature dependence of inorganic nitrogen uptake: reduced affinity for nitrate at suboptimal temperatures in both algae and bacteria**. *Appl Environ Microbiol* 1999, **65**(6):2577-2584.
80. Lovley DR, Chapelle FH: **Deep Subsurface Microbial Processes**. *Reviews of Geophysics* 1995, **33**(3):365-381.
81. Lovley DR, Phillips EJ: **Requirement for a Microbial Consortium To Completely Oxidize Glucose in Fe(III)-Reducing Sediments**. *Appl Environ Microbiol* 1989, **55**(12):3234-3236.

82. Hansen LK, Jakobsen R, Postma D: **Methanogenesis in a shallow sandy aquifer, Rømø, Denmark** *Geochimica et Cosmochimica Acta* 2001, **65**(17):2925-2935.
83. Kuivila K, Murray J, Devol A, Novelli P: **Methane production, sulfate reduction and competition for substrates in the sediments of Lake Washington**. *Geochimca et Cosmochimca Acta* 1989, **53**:409-416.
84. Crill PM, Martens CS: **methane prouction from bicaronate and acetate in an anoxic marine sediment** *Geochimca et Cosmochimca Acta* 1986, **50**:2089-2097.
85. Chapelle FH, Lovley DR: **Rates of Microbial Metabolism in Deep Coastal Plain Aquifers**. *Appl Environ Microbiol* 1990, **56**(6):1865-1874.
86. Lovley DR, Klug MJ: **Model for the distribution of sulfate reduction and methanogenesis in freshwater sediments**. *Geochimica et Cosmochimica Acta* 1986, **50**:11-18.
87. Yabusaki SB, Fang Y, Long PE, Resch CT, Peacock AD, Komlos J, Jaffe PR, Morrison SJ, Dayvault RD, White DC *et al*: **Uranium removal from groundwater via in situ biostimulation: Field-scale modeling of transport and biological processes**. *Journal of contaminant hydrology* 2007, **93**(1-4):216-235.
88. Petrie L, North NN, Dollhopf SL, Balkwill DL, Kostka JE: **Enumeration and characterization of iron(III)-reducing microbial communities from acidic subsurface sediments contaminated with uranium(VI)**. *Appl Environ Microbiol* 2003, **69**(12):7467-7479.
89. Holmes DE, O'Neil RA, Vrionis HA, N'Guessan L A, Ortiz-Bernad I, Larrahondo MJ, Adams LA, Ward JA, Nicoll JS, Nevin KP *et al*: **Subsurface clade of *Geobacteraceae* that predominates in a diversity of Fe(III)-reducing subsurface environments**. *ISME J* 2007, **1**(8):663-677.
90. Strycharz S: Personal Communication.
91. Pfeiffer T, Bonhoeffer S: **An evolutionary scenario for the transition to undifferentiated multicellularity**. *Proc Natl Acad Sci U S A* 2003, **100**(3):1095-1098.
92. Pfeiffer T, Schuster S: **Game-theoretical approaches to studying the evolution of biochemical systems**. *Trends Biochem Sci* 2005, **30**(1):20-25.
93. Holmes DE, Finneran KT, O'Neil RA, Lovley DR: **Enrichment of members of the family *Geobacteraceae* associated with stimulation of dissimilatory metal reduction in uranium-contaminated aquifer sediments**. *Appl Environ Microbiol* 2002, **68**(5):2300-2306.
94. Holmes DE, Bond DR, O'Neil RA, Reimers CE, Tender LR, Lovley DR: **Microbial communities associated with electrodes harvesting electricity from a variety of aquatic sediments**. *Microb Ecol* 2004, **48**(2):178-190.
95. Holmes DE, O'Neil RA, Chavan MA, N'Guessan LA, Vrionis HA, Perpetua LA, Larrahondo MJ, DiDonato R, Liu A, Lovley DR: **Transcriptome of *Geobacter uraniireducens* growing in uranium-contaminated subsurface sediments**. *ISME J* 2009, **3**(2):216-230.
96. Methe BA, Webster J, Nevin K, Butler J, Lovley DR: **DNA microarray analysis of nitrogen fixation and Fe(III) reduction in *Geobacter sulfurreducens***. *Appl Environ Microbiol* 2005, **71**(5):2530-2538.

97. Lovley DR, Klug MJ: **Sulfate Reducers Can Outcompete Methanogens at Freshwater Sulfate Concentrations**. *Appl Environ Microbiol* 1983, **45**(1):187-192.
98. Balba MT, Nedwell DB: **Microbial-Metabolism of Acetate, Propionate and Butyrate in Anoxic Sediment from the Colne Point Saltmarsh, Essex, Uk**. *Journal of General Microbiology* 1982, **128**(Jul):1415-1422.
99. Pianka ER: **On r and K selection**. *Amer Naturalist* 1970, **104**:592-597.
100. Gudelj I, Beardmore RE, Arkin SS, MacLean RC: **Constraints on microbial metabolism drive evolutionary diversification in homogeneous environments**. *J Evol Biol* 2007, **20**(5):1882-1889.

Appendix I. Thesis Outline

This document is a Masters of Applied Science thesis submitted to the Graduate Department of Chemical Engineering at the University of Toronto. This thesis primarily focuses on the development of the Dynamic Multi-species Metabolic Modeling (DMMM) framework. A large portion of this thesis is adapted from the research paper "*Genome-Scale Dynamic Modeling of the Competition Between Rhodoferax and Geobacter in Anoxic Subsurface Environments*" [1]. This fulfills a special requirement of University of Toronto Chemical Engineering Graduate program, which allows research papers to be submitted as thesis by adding sufficient background information. Since the research paper is submitted to the International Society of Microbial Ecology Journal, it is intended for a microbial biology audience instead of an engineering one. The adaptation is aimed to make the document more suitable for an engineering audience.

The main body of this thesis includes five chapters. Chapter 1 provides an introduction to uranium bioremediation as well as our motivation in developing a computational model of the uranium contaminated subsurface community. The objective of this thesis is discussed at the end of this chapter. Chapter 2 provides a more detailed introduction to metabolic modeling, as well as our reasons for developing the Dynamic Multi-species Metabolic Modeling (DMMM) framework. Chapter 3 describes the DMMM framework as well as its advantages comparing to other modeling techniques as well experiments. Chapter 4 describes the methods by which we applied the DMMM framework to the

Geobacter and *Rhodoferax* community. Chapter 5 describes and discusses the simulation results. Chapter 6 summaries this work and provides some future recommendations.

Section 1.3 of Chapter 1, as well as Chapters 3-6 are adapted from the research paper "*Genome-Scale Dynamic Modeling of the Competition Between Rhodoferax and Geobacter in Anoxic Subsurface Environments*" [1]. Chapter 2 is adapted from the review paper "*Constraint-Based Metabolic Model: an Interdisciplinary Tool for Improving Biotechnology Applications*" [2]. Kai Zhuang is the first author of both papers, and only the portions authored by Kai Zhuang have been used in this adaptation.

While Kai Zhuang is the sole author of this document, the work of many collaborators were instrumental in the development and testing of the DMMM framework as well as its application to the *Geobacter* and *Rhodoferax* subsurface community. Their contributions are clarified and acknowledged here:

The Dynamic Multi-species Metabolic Modeling (DMMM) framework is developed and coded using MATLAB by Kai Zhuang. In order to apply the DMMM framework to the *Geobacter* and *Rhodoferax* community, the genome-scale metabolic models as well as many experimental parameters were required. The metabolic model of *Geobacter sulfurreducens* has been previously published [3]. Based on the experimental work of Bahareh Sayyar, Kai Zhuang has modified the nitrogen fixation stoichiometry of the model. The *Rhodoferax ferrireducens* model is developed by Jun Sun and is described in a submitted manuscript [4]. Kai Zhuang is a coauthor of this manuscript; he is responsible for the calculation of the electron transport chain and maintenance energy

stoichiometry. The acetate uptake parameters of *G. sulfurreducens* were experimentally measured by Hanno Richter and modified by Kai Zhuang. The procedure is described in a submitted manuscript [5]. The 16S rRNA data from 2007 *in situ* acetate injection experiment at Rifle Colorado is acquired from Paula Mouser through Derek Lovley. All other parameters not mentioned are derived/calculated/measured by Kai Zhuang

Appendix II. List of Simulation Parameters

Acetate Uptake Parameters

G. sulfurreducens		
$K_{s,1}$	0.012 mM	[5, 78]
$K_{s,2}$	0.0167 mM	
$K_{s,3}$	0.777 mM	
$V_{max,1}$	2.67 mmol/gDW/hr	
$V_{max,2}$	2 mmol/gDW/hr	
$V_{max,3}$	13.33 mmol/gDW/hr	

R. ferrireducens		
K_s	0.012 mM	Assumed to be the same as *G. sulfurreducens*
V_{max}	1.71 mmol/gDW/hr	[20]

Ammonium Uptake Parameters

G. sulfurreducens		
K_s	0.074 mM	Assumed to be the same as E. coli [79]
V_{max}	0.468 mmol/gDW/hr	Calculated by FBA

R. ferrireducens		
K_s	0.074 mM	Assumed to be the same as E. coli [79]
V_{max}	0.127 mmol/gDW/hr	Calculated by FBA

Simulations under Natural Conditions

$[Fe_3]_{init}$	10 mM	[7, 15, 87, 88]
Acetate Turnover Rate	00-0.54 μM/hr	[82-86, 97, 98]
Ammonium Concentration	0 – 400 μM	[16]
$[G.\ sulfurreducens]_{init}$	10^5 cells/L	[89]
$[R.\ ferrireducens]_{init}$	10^5 cells/L	[89]
Dilution rate	0.00141 hr^{-1}	Calculated based on geometry [7, 15, 87, 88]

Simulations During Acetate Addition

$[Fe_3]_{init}$	10 mM	[7, 15, 87, 88]
Acetate Injection Rate	4.2 - 7 μM/hr	[7, 15]
$[NH_4]_{init}$ (excess)	400 μM	[16]
$[NH_4]_{init}$ (limiting)	5 μM	[16]
[*G. sulfurreducens*]$_{init}$	10^5 cells/L	[89]
[*R. ferrireducens*]$_{init}$	10^5 cells/L	[89]
Dilution rate	0.00141 hr^{-1}	Calculated based on geometry[7, 15]

Cell Number to Cell Mass Conversion

Mounir Izallalen has calculated the average mass of *G. sulfurreducens* to be 10^{-12} g per cell using the following method [1]:

1. Grow cells in large volumes (>1L).
2. Stop growth in mid exponential phase.
3. Perform cell count using fluorescent microscopy.
4. Collect dry cell fractions using centrifuge method. Measure Dry Cell Mass with a spring of sufficient precision.
5. Calculate the conversion factor between Dry Cell Mass and Cell Number.

The average volume of *G. sulfurreducens* and *R. ferrireducens* are calculated based on the published dimensions for these organisms [18, 20]. Cells are assumed to be rod shaped. *R. ferrireducens* is calculated to be 6.25 times the size of *G. sulfurreducens*. Therefore, the average mass of *R. ferrireducens* is 6.25×10^{-12} g per cell.

Appendix III. Nomenclature

DMMM	Dynamic Multi-species Metabolic Modeling framework
MASC	Masters of Applied Science
ODE	Ordinary Differential Equations
U(VI)	Uranium (VI)
U(IV)	Uranium (IV)
Fe(III)	Iron (III), ferric iron
Fe(II)	Iron (II), ferrous iron
rRNA	ribosomal RNA
CBM	Constraint-Based Model (in this document, CBM refers specifically to a constraint-based **metabolic** model.)
Exchange flux	An exchange flux is a reaction flux where the metabolite either moves from the outside to the inside of the cell, or vice versa. (Unit: mmol/gDW/hr)
Uptake rate	The rate a metabolite is absorbed into the cell, equal to the exchange flux. (Unit: mmol/gDW/hr)
Production rate	The (overall) rate of production of a metabolite. (Unit: mM/hr)
Consumption rate	The (overall) rate of consumption of a metabolite. (Unit: mM/hr)

Note: the concept of uptake rate and consumption rate is similar and should be distinguished. These two rates are mathematically equivalent if and only if there is only one microbial species within the community being modeled. The "uptake rate" of metabolite i by species j is equal to the exchange flux v_i^j, whereas the "consumption rate" of metabolite i is equal to the summation of all exchange fluxes relevant to metabolite i, or $\sum v_i^j X^j$ over the range of j ($1 \leq j \leq$ number of microbial species).

Acetate turnover rate	The rate at which acetate is been generated in the natural environment. The primary source of acetate prior to acetate injection is from fermentation, and the "acetate turnover rate" describes this rate. (Unit: mM/hr)
Cell Concentration	Number of cells per unit volume (cells/L)
Physical Density	Here, physical density refers to the mass of the intracellular contents per unit volume (g/L).

Appendix IV. Mathematical Symbols

μ	Specific growth rate (Unit: g new cells/g cells/hr)
r^D	Specific death rate (Unit: g dead cells/g cells/hr)
c^T	FBA objective column This column chooses which reaction flux(es) is the target of optimization.
A	The stoichiometric matrix representation of the chemical reaction network
v	the vector of reaction fluxes (Unit: mmol/gDW/hr)
v^{max}	the vector of maximum reaction fluxes (Unit: mmol/gDW/hr)
v^{min}	the vector of minimum reaction fluxes (Unit: mmol/gDW/hr)
i	the ^{i}th metabolite within A
j	the ^{j}th organisms of the community
S_i	the ^{i}th substrate
q^S	uptake rate of substrate S (Unit: mmol/gDW/hr)
m^S	maintenance requirement of substrate S (Unit: mmol/gDW/hr)
Y	biomass yield (Unit: gDW/mmol)
m^{ATP}	Non-growth-related ATP maintenance flux (Unit: mmol/gDW/hr)
V_i^{max}	Maximum specific uptake rate of metabolite i (Unit: mmol/gDW/hr)
V_i	specific uptake rate of metabolite i (Unit: mmol/gDW/hr)
N	population number (in Verhulst equation)

Appendix V. List of Equations and Equation Sets

Equation 1. Original FBA formulation

$$\text{maximize } z = c^T v$$

$$\text{subject to } Av = 0$$

$$v^{\min} \le v \le v^{\max}$$

Equation 2. dFBA formulation

$$\frac{dX}{dt} = \mu X$$

$$\frac{dS_i}{dt} = A_i v_i X$$

$$\text{Maximize } \mu = c^T v$$

$$\text{subject to } Av = 0$$

$$v^{\min} \le v \le v^{\max}$$

$1 \le i \le$ to number of metabolites

Equation 3. DMMM framework formulation

$$\frac{dX_j}{dt} = \mu_j X_j$$

$$\frac{dS_i}{dt} = \sum^{j} A_i{}^j v_i{}^j X_j$$

Maximize $\mu_j = c^T v_j$

subject to $A_j v_j = 0$

$$v_j{}^{\min} \le v_j \le v_j{}^{\max}$$

$1 \le$ i $\le$ to number of metabolites

$1 \le$ j $\le$ to number of microbial species

Equation 4. Using Michaelis –Menten kinetics to calculate dynamic flux constraints

$$V_{i,\text{constraint}} \le V_i^{\max} \bullet \frac{\mathrm{S}_i}{\mathrm{S}_i + \mathrm{K}^i{}_s}$$

Equation 5. Rate of change of biomass j

$$\frac{dX^j}{dt} = \mu^j X^j$$

Equation 6. Rate of change of metabolite i

$$\frac{dS_i}{dt} = \sum^{j} v_i{}^j X_j$$

Equation 7. Calculation of Cell Death based on Maintenance Requirement

$$r^D = (q^S - m^S)Y$$

Equation 8. Single Monod Model

$$\mu = \mu^{\max} \bullet \frac{[S]}{[S] + K_s}$$

Equation 9. Double Monod Model

$$\mu = \mu^{\max} \bullet \frac{[S_1]}{[S_1] + K_{s_1}} \bullet \frac{[S_2]}{[S_2] + K_{s_2}}$$

Equation 10. General Monod Model

$$\mu = \mu^{\max} \bullet \prod_{1}^{i} \frac{[S_i]}{[S_i] + K_{s_i}}$$

Equation 11. Calculation of Acetate Uptake Constraint of *Geobacter sulfurreducens*

$$V_{ac}^{Gs} = \frac{13.3[Acetate]}{[Acetate] + 0.77} + \frac{2[Acetate]}{[Acetate] + 0.167} + \frac{2.67[Acetate]}{[Acetate] + 0.012}$$

Equation 12. Calculation of Acetate Uptake Constraint of *Rhodoferax ferrireducens*

$$V_{ac}^{Rf} = \frac{1.71[Acetate]}{[Acetate] + 0.012}$$

Equation 13. Calculation of Ammonium Uptake Constraint of *Geobacter sulfurreducens*

$$V_{NH_4}^{Gs} = \frac{0.468[Ammonium]}{[Ammonium] + 0.074}$$

Equation 14. Calculation of Ammonium Uptake Constraint of *Rhodoferax ferrireducens*

$$V_{NH_4}^{Rf} = \frac{0.127[Ammonium]}{[Ammonium] + 0.074}$$

Equation 15. *Geobacter* fraction formula

$$\textit{Geobacter}\ \text{fraction} = \frac{\text{Number of } G.\ \textit{sulfurreducens}}{\text{Number of } G.\ \textit{sulfurreducens} + \text{Number of } R.\ \textit{ferrireducens}}$$

Equation 16. Verhulst Equation

$$\frac{dN}{dt} = rN\left(1 - \frac{N}{K}\right)$$

Appendix VI. Disambiguation: r-Y tradeoff

A major find of this thesis is that the competition between *Geobacter* and *Rhodoferax* species is to a large part determined by the rate vs. yield (r-Y) tradeoff. The rate vs. yield tradeoff stems from the 2nd law of thermodynamics – in any non-equilibrium system, the entropy increases. This implies that for any organism to escape "entropy death", the organism must continue to dissipate energy (mostly through chemical reactions). Higher energy dissipation allows faster chemical reactions, but leaves less energy to be converted into biomass, hence creating the tradeoff. The r-Y tradeoff was discussed in depth in Section 2.2.

The r-Y tradeoff is closely related to but distinct from the r-K selection mechanism in evolutionary ecology. The r-K selection mechanism refers to a general evolutionary tradeoff: given limited resources, the r-strategists maximize the quantity of offspring, whereas the K-strategists maximize the quality of offspring [99]. Here, r and K refer to growth rate and carrying capacity of the environment in the Verhulst equation of population dynamics. N is the population number of the organisms.

$$\frac{dN}{dt} = rN(1 - \frac{N}{K}) \tag{16}$$

Although both r-Y tradeoff and r-K selection are evolutionary equivalents of the Tragedy of Common problem in economics, the nature of the tradeoffs are very different. The r-Y tradeoff is based in thermodynamics and exists at the level of chemical reactions, whereas the r-K selection exists at the level of descriptive ecology, and should be viewed as an integrated description of multiple tradeoffs, which could have its root in the r-Y tradeoff.

Another ambiguity could arise from the uptake rate vs. substrate affinity tradeoff. While the physiological basis of this tradeoff is still unknown, there is clear evidence for its existence [100]. With respect to microbiology, it is possible that the observed r-K selection mechanism is the integrative effect of both r-Y tradeoff and rate vs. affinity tradeoff. It is important for scientists to distinguish the physiological/mechanistic tradeoffs from the descriptive r-K selection mechanism.

Appendix VII. Applications of DMMM

As of July 7, 2009, the DMMM framework was used to create the dynamic community metabolic models of 4 microbial communities. These includes:

1. *Geobacter sulfurreducens* and *Rhodoferax ferrireducens* (Kai Zhuang)
2. *Geobacter sulfurreducens* and *Geobacter metallireducens* (Zhao Jiao)
3. *Geobacter sulfurreducens* and acetate-oxidizing sulfate reducers (Kai Zhuang)
4. *Geobacter sulfurreducens*, *Desulfovibrio vulgaris*, and acetate-oxidizing sulfate reducers (Kai Zhuang)

Names in bracelets are the lead developers of the respective community model.